



Flame-Based Technologies and Reactive Spray Deposition Technology for Low-Temperature Solid Oxide Fuel Cells: Technical and Economic Aspects

Radenka Maric, Justin Roller, and Roberto Neagu

(Submitted December 8, 2010; in revised form March 7, 2011)

The economic and technical breakthroughs in solid oxide fuel cell (SOFC) for commercial success still depend on high-quality manufacture, reliability, efficiency, and must have an acceptable cost when compared to competing technologies. The application of flame-based technologies as a one-step deposition technique for SOFC component manufacture has potential to reduce both cost and production time. In this article, cells produced by flame processes have been reviewed with emphases placed on the Reactive Spray Deposition Technology technique. Various experimental methods and examples for the synthesis of porous electrodes and dense electrolytes are reviewed. The studies focus on determining the range of the flame conditions under which each of the individual cell components for low temperature SOFC applications ~600 °C could be successfully deposited.

Keywords direct deposition methods, flame spray, flame spray pyrolysis, flame-based process, reactive spray deposition, solid oxide fuel cell, thin film technology

1. Introduction

The main barriers for the introduction of solid oxide fuel cell (SOFC)-based systems for combined heat and power generation and auxiliary power for transport applications are the lifetime of stacks and the cost of the systems. SOFCs can deliver very high efficiency (80% or better, in combined heat and power applications) which makes them competitive with other industrial energy sources (Ref 1). When fueled by hydrocarbons, these devices can produce lower greenhouse gas emissions per unit energy than competing industrial energy sources (due to their high efficiency). The CO₂ waste stream thus produced is purer and therefore more amenable to carbon sequestration and enhanced oil recovery, two important elements in the emerging energy landscape world-wide.

A critical cost factor arises from the very high temperature (800 to 1000 °C) at which present SOFCs must operate (Ref 2). Unfortunately, thermally activated

degradation mechanisms that limit lifetime are accelerated at these higher temperatures (sintering of electrodes, stability of phases, and mutual reactivity of components) and these will be slowed down significantly by decreasing the operation temperature (Ref 3, 4).

Presently, the goal of SOFCs is to reduce both stack and system costs to make them competitive with existing technologies. The reduction in cost is typically associated with the reduction of operation temperature, simplified stack design, lower power electronics cost, and increasing the ease of system integration (Ref 4-6).

Operating temperature can substantially be reduced to around 600 °C by advanced material design, properties, and processing (Ref 7). Some of the benefits of a reduced temperature include: (1) better thermal integration with fuel reformers and sulfur removal systems, (2) reduced material issues such as less thermal stress and more material flexibility, (3) lower heat loss, (4) shorter time to achieve operating temperature, and (5) less corrosion (Ref 8, 9).

Much of the present research is focused on developing SOFC materials for use at 600 °C, which is low enough that alternative materials become available to significantly reduce cost (Ref 7, 10-13). Further reduction in operating temperature to 500 °C could yield even greater cost savings (Ref 14, 15). The reduced operating temperature would also improve mechanical robustness, reduce thermal stresses, and reduce chemical interactions among the various components. However, operating the SOFC at low temperature increases the performance requirements for the cell components. In general, use of Ni-Y₂O₃-stabilized ZrO₂ (Ni-YSZ)-based porous cermet anodes as the support is the favored design for low-temperature SOFCs. Ni-YSZ anodes have excellent electrocatalytic activity for

Radenka Maric and **Justin Roller**, Department of Chemical, Materials and Biological Engineering, University of Connecticut, Storrs, CT; **Radenka Maric**, Connecticut Center for Clean, Energy Engineering, Storrs, CT; and **Roberto Neagu**, Institute for Fuel Cell Innovation, National Research Council of Canada, Ottawa, Canada. Contact e-mails: radenka.maric@uconn.edu and Justin.roller@uconn.edu.



H₂ and other hydrocarbon fuel oxidation reactions which occur at the triple phase boundary (TPB) among Ni, YSZ, and gaseous H₂ (Ref 12, 16, 17).

The major disadvantage of a lower operating temperature for SOFC stacks is the lower power density. This is mainly attributed to an increased ohmic resistance, increased polarization resistances, and losses over the interface between the cell and the interconnects. These losses between the interface and the interconnect occur as corrosion scales. Contact coatings are often applied to reduce the formation of scales, but these coatings behave like semiconductors, in that their electronic conductivity is inversely proportional to the temperature and thus lower temperatures reduce electrical conductivity in these layers.

Development challenges are focused on the development of new highly optimized cathodes and anodes for reducing polarization and ohmic losses and electrolyte materials with high ionic conductivity at low temperature. The ionic conductivity of the current generation of ceramic materials is directly proportional to temperature, which makes using current state of the art materials inadequate for LT-SOFC applications (Ref 18). Materials with adequate electrical conductivity at lower temperatures are being developed. The anode materials have to withstand (transient) oxidizing conditions (redox cycling resistance), should be tolerant to sulfur and should not strongly catalyze carbon deposition from carbon-containing fuels (Ref 19).

Currently, the most common solid oxide electrolyte is yttria-doped zirconia. To reduce the ionic resistance of these components the yttria content is varied between 8 and 10 mol% (instead of the usual 3%), other dopants such as (Sc) are applied and the thickness is reduced. These options are, however, inadequate for achieving the required low resistivity at operating temperatures around 600 °C. Moreover, thin electrolytes decrease the mechanical strength of cell, which is highly undesirable with respect to reliability and robustness of SOFC stacks. One avenue of research toward operation at LT SOFC temperatures is the investigation of nanomaterials for use as the ionic conducting electrolyte membrane. Improved ionic conductivity has been associated with the use of nanostructured materials as electrolytes (Ref 20-22). Alternative electrolyte compositions like doped ceria and lanthanum strontium gallium magnetite (LSGM) have been investigated, but these materials suffer from chemical instability at the higher operating temperatures (which may be reduced at temperatures of around 600 °C) and poor mechanical reliability.

Another challenge generated by lowering the operation temperature of the fuel cell is that the cathode kinetics are slowed appreciably. Almost 20 years ago, B.C.H. Steele emphasized the importance of oxygen exchange kinetics in determining the magnitude of cathode resistivity values (Ref 23, 24). Subsequent publications have discussed semi-quantitatively the relative roles of microstructural features on oxygen surface and bulk diffusion D^* (cm⁻²/s), and oxygen surface exchange kinetics k (cm/s) (Ref 25, 26). More recent publications have provided a detailed

quantitative interpretation of the behavior of porous mixed conducting oxygen electrodes which integrate information about the various macroscopic pathways available for the cathodic reduction of oxygen (Ref 27). The cathode is also very sensitive to microstructure changes and the effect is particularly evident at lower temperatures.

There is also a drive to reduce the cost of SOFCs by supporting the cell on metallic cell interconnects rather than using expensive rare-earth ceramics, such as LaCrO₃, that are traditionally used as interconnect materials for high temperature SOFCs, or onto anode supports, which use thicker layers of a more expensive material (Ref 28). Supporting the cells mechanically on the cheaper metallic interconnects allows the use of thinner layers of the more expensive anode, cathode, and electrolyte layers (Ref 29-31). This decreased thickness of active layers both lowers the cost of the cells and increases performance by reducing barriers to diffusion and conductivity. The history of SOFC architecture development is presented in Fig. 1. Currently, researchers in Europe are very focused on development of the metal-supported concept.

Another important aspect to consider in materials development for SOFCs is the role that fabrication and processing (i.e., heating and sintering regime) will play in the performance of the cell. Moreover, the fabrication route will play an important role on the size and the impurities of the particles that make up SOFC cell components. With the advent of nanotechnology development, interest in nanoparticles produced by flame-based processes and other processing methods increased with a focus on size effect of nanostructured material. The reason for this approach is a high surface to volume ratio when compared to micron-sized particles. For particles of 4 nm size, half of the molecules forming the nanostructure are actually at the surface. This causes a dramatic change in the physical and chemical properties when compared to bulk materials and changes, e.g., the melting temperature, the mechanical properties, as well as catalytic behavior that will directly influence the performance of the SOFC. Nanostructured SOFC components can be fabricated via routes such as electrochemical vapor deposition (EVD), chemical vapor deposition (CVD), physical vapor deposition (PVD), sol-gel, RF-sputtering, spin coating, slurry spraying, liquid flame spray, plasma spray, and screen-printing (Ref 32-35).

The driving force in SOFC material development is a low-cost, rapid processing method that can be done in one continuous process without the need for long sintering times at elevated temperatures. The choice of an appropriate thin film deposition technique is strongly influenced by the material to be deposited and the desired film quality and available budget (Ref 36). Each technique has its advantages and disadvantages, which usually involve high costs such as use of a vacuum, long sintering steps, and/or large energy requirements. The use of long sintering steps at higher temperatures must be avoided when co-firing the cathode and electrolyte components to retard formation of unwanted insulating oxides. Various new production processes for SOFCs are currently under development. Thermal and plasma spraying are common

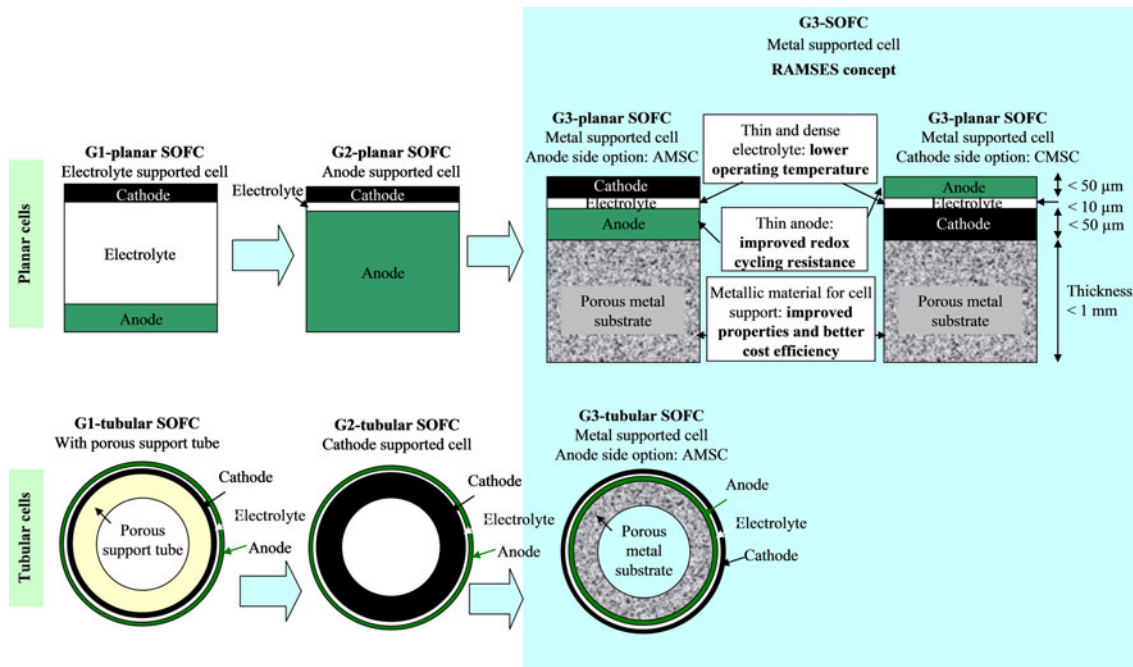


Fig. 1 Scheme illustrating the basic development approach and evolution of SOFC architectures for the EU-framework 7 program

techniques commonly used to produce films of SOFC electrode/electrolyte materials but not for proton exchange membrane (PEM)-type fuel cells. Plasma spraying usually involves passage of a solid powder to a direct current or alternating current plasma, subsequent melting of the solid particles and formation of splats of material on the substrate. The length of time in the plasma depends on the type of torch, gas flows, and plasma shaping devices (i.e., cooling shrouds). Plasma spray process, especially low-pressure plasma spraying, is a promising process for cell manufacturing because of its fast deposition rate. Atmospheric plasma spraying (APS) has been widely investigated for the production of dense electrolyte layers (Ref 35, 37-40). However, the high porosity of APS sprayed electrolyte layers results in a high gas permeability and consequently a low open circuit voltage (OCV) of the SOFC (Ref 38). Recently, the use of suspension and solution injection came into consideration to make very fine particles suitable for processing (Ref 40). With some success, such suspensions have been applied with DC torches used in the open atmosphere but the spray distance had to be very short and, therefore, local overheating of the substrate took place. The density of the YSZ electrolyte was reported to be less than 90% (Ref 41). Nevertheless, means have to be developed to make the electrolyte layer as dense as possible either by process improvement or by postprocessing.

Moving to lower SOFC temperatures, the electrolyte needs to be very thin and dense in order to obtain a high power density and high fuel utilization. From this perspective the plasma spray process still needs improvement to make a dense and thin electrolyte layer. Moreover, Hui et al. (Ref 37, 42) reported that APS faces another challenge such as insufficient porosity of the electrode. Alternatively,

lower energy technologies have been explored as possible alternate deposition techniques to plasma spraying. Worldwide research has led to the development of many similar techniques for open atmosphere lower energy flame depositions. Research at the National Research Council of Canada Institute for Fuel Cell Innovation (NRC-IFCI) has developed two cost effective techniques for spray pyrolysis, electrostatic spray deposition, and pneumatic spray deposition. Researchers used both methods to deposit samaria-doped ceria (SDC), YSZ electrolytes, and lanthanum strontium cobalt ferrite (LSCF) cathodes on cermet or metal-supported anodes for SOFCs operated at reduced temperature (Ref 11). The main advantages of spray pyrolysis depositions are simplicity of the apparatus, low cost of the process, and the good productivity of the technique on larger scales (Ref 43, 44).

In addition, spray pyrolysis deposition has a number of advantages: (1) it offers an extremely easy way to dope films with virtually any element in any proportion by merely adding it in some form to the precursor solution (Ref 45, 46); (2) unlike closed vapor deposition methods, spray pyrolysis deposition does not require high-quality targets and/or substrates or does it require a vacuum at any stage, which is a great advantage if the technique is to be scaled up for industrial applications; (3) the deposition rate and the thickness of the films can be easily controlled over a wide range by changing the spray parameters, thus eliminating the major drawbacks of other chemical methods such as spin coating which produces films of limited thickness; (4) operation at moderate temperatures (typically 300-600 °C); (5) dense or porous film can be deposited when using different spray parameters; (6) by changing the composition of the spray solution during the spray process layered films and films having composition



gradients throughout the thickness can be made (Ref 47). However, after spraying the layer a sintering process is still required and the cost of sintering cannot be eliminated along with the challenges associated with formation of unwanted insulators.

Researchers at NRC-IFCI have also developed an open atmosphere flame-based process called Reactive Spray Deposition Technology (RSDT) for depositing both high-temperature SOFC and low-temperature PEM layers (Ref 48-50). For SOFC applications, the layers are deposited directly onto an anode and metal support. The process temperature is 700-1200 °C and this addresses sintering issues by removing the necessity of co-firing the cathode and electrolyte. RSDT has the potential to penetrate the SOFC market because of the enormous cost savings advantage, coupled with the ability to coat large surface areas with multi-element compounds. The cost advantages are the result of two factors. First, the RSDT process uses low vapor pressure precursors that are generally one hundred times less expensive than those used by currently available technologies like chemical vapor deposition (CVD). Secondly, the capital equipment costs for a functional RSDT system is ten times less expensive than a CVD system.

In laboratory scale development at NRC, the RSDT technique has been successfully used to deposit porous cathodes, porous anode functional layers, dense electrolytes, dense blocking layers on substrates up to 80 × 80 mm, interconnect coatings, and depositions on metal substrates. The results confirm that the technique is able to produce different microstructures in one processing step just by adequately tuning the instrument. Moreover, the technique has proven to be stable, controllable, and reproducible for different precursor chemistries. For industrial applications, it has been estimated that the SOFC (approximately 300 cm²) will have to be produced with controlled structures at a rate of one cell per second to meet commercial volumes.

For RSDT to meet this industrial target either the nozzle has to be enlarged or an array of multiple nozzles must be configured.

This article reviews recent developments in flame generation of the thin electrolytes, and porous electrodes with an emphasis on application of RSDT for low temperature SOFC development. The main focus of these research efforts is to obtain higher reliability and lower production costs. These challenges are addressed by lowering the operating temperature through thinner electrolyte layers and depositing high surface area anodes and cathodes. Because of the depth and breadth of the flame processes, this review is restricted to the quality of the coating and performance of the layers and cell and does not address basic flame and aerosol science and technology in general.

2. Flame-Based Processing of Materials for SOFC Thin Film Deposition

Today, flame technology creates new materials for catalyst, composite, and other applications and accounts

for about 90% by sale and volume of fine particles made in the gas phase (Ref 51-54). According to the volume of literature on the subject thermal spray and plasma spraying are both techniques more commonly seen in the literature to produce films for SOFC electrode/electrolyte materials as opposed to flame-based depositions (Ref 55-58). Alternative, lower energy technologies have been explored that possibly promise alternative deposition techniques to plasma spraying. Researchers around the world have developed several similar techniques for open atmosphere lower energy flame depositions (Ref 35, 36, 47, 52, 59-68). Variations of the flame process include RSDT in Canada at the NRC-IFCI, flame-assisted vapor deposition (FAVD) in London at the Imperial College of London, oxy-acetylene combustion-assisted aerosol-chemical vapor deposition (OCAACD) at the University of Science and Technology of China and combustion chemical vapor deposition (CCVD) in the United States at nGimat, Georgia Tech and North Carolina State University (Ref 69-74).

The flame-based process can be either a mainly physical process, when a suspension of fine oxide particles in a flammable liquid carrier is utilized, or physical and chemical when metal salts in a flammable solvent mixture are used as educts for the ceramic coating formation. The atomization of the spray can be accomplished by nozzles that atomize using ultrasonics, air shear, liquid pressure, and heat or a combination of energy inputs. Precursor solutions containing the metal reactants required in the deposited film are pumped under pressure to the nozzle by use of a syringe or HPLC pump. In addition, some techniques feed the precursors to the nozzle as an aerosol and the nozzle is not used in the atomization process. In yet another version of the technique, a dissolved liquefied gas is added to the precursor solution to aid in atomization through a technique known as supercritical fluid atomization. Regardless of the nozzle type, the atomized spray is then combusted by an ignition source such as a single pilot flame from a point source or a ring of pilots surrounding the exit of the nozzle. An optimal ignition point must be chosen since igniting too close to the exit of the nozzle results in a fuel-rich mixture that does not burn easily, while igniting too far away results in an oxidant-rich mixture. Pilot gases consist of methane and oxygen or an oxy-acetylene-type gas. A sprayed precursor breaks into droplets that rapidly evaporate and start to decompose into a primary gas phase compounds. Consumption of the gaseous precursors can proceed either by gas or surface reactions, or by both. The decomposition kinetics can also interact with the kinetics of combustion, e.g., via radical reactions. Radicals, intermediates, and product molecules are formed which nucleate into clusters; the clusters thermal stability determines in many cases the future evolution of the particle or film forming process. The cluster can grow either at the gas kinetic collision rate or by addition of the monomers to the cluster surface. The coalescence of the clusters is normally very fast and can be in range of 10⁻² to 10⁻⁴ s (Ref 75).

Depositions onto substrates usually occur by impinging the flame on the desired substrate and allowing the

reaction to occur long enough for the desired thickness of film. During deposition, when typical particle diameters become larger than several nanometers, the future development of the particle is determined by surface growth and by the interdependence of coagulation and coalescence. A coalescence rate shows a strong dependence on both the size of the clustered particles, concentration, and temperature of the flame. If a small nanoparticle size is desired then the flame should be quenched to prevent further agglomerate growth. This has been successfully demonstrated by making proton exchange catalysts with narrow particle size distributions of 3-5 nm (Ref 48, 76). Practical large-scale production of unagglomerated particles is possible through careful engineering control of the residence time, the quench rate, and the medium of quenching, i.e., water or gas. Feedstock properties, residence time, solute concentration, and temperature of the flowing gas are all key processing inputs that determine the morphology and crystallinity of the deposited films.

If a nanostructured or dense film is desired then the flame should penetrate the boundary layer of the substrate. Longer flames, larger stand-off distances, and higher concentrations of precursor material favor nucleation of particles and agglomeration prior instead of growth from the vapor phase directly on the substrate. Agglomeration instead of growth from the film results in a powdery particles with poor adhesion. Care must be taken to prevent thermal shock to the substrate by controlling the heat up and cool down to deposition temperatures. This is generally done by heating the substrate from the back by resistive heaters or by another flame. Additionally, the heat up and cool down must be performed without the reactive precursors present so that a constant deposition temperature is maintained during film growth. Alternatively, the flame can be directed at a sheet of cooling air, water or a cooled metal surface for collection of powder particles instead of a growing film.

One advantage of flame processing is that multi-layer and/or functionally graded materials can be deposited in one single process by simply changing the precursor material and deposition conditions. Changing of the precursor material in a controlled manner can be accomplished using existing HPLC technology for gradient elution. Functionally graded cathode materials have been explored by Liu and researchers at Georgia Tech (Ref 73).

2.1 Different Flame Processes

This section gives an overview of the most relevant thin film deposition flame techniques for SOFC applications. Researchers around the world have developed varied systems for deposition by flame-based reactors. This section will compare and contrast the different methods of deposition used for SOFC applications. Differences generally lie in degree of atomization, type of atomizer, solution injection geometry, and the fuel used in the flame. For instance, Xu et al. (Ref 72) at NC State used a TQ-20-A2 Meinhard nebulizer for atomizing and a single point pilot flame for ignition of the atomized spray. In addition, a heating torch was applied to the back of the substrate

holder to minimize the thermal gradient between the front and back of the substrate.

Meng and researchers (Ref 70, 71) at the University of Science and Technology in China used a modified oxy-acetylene torch with a 2 mm diameter and fitted at an angle of 45° to the substrate. Precursors were supplied to the torch by means of an ultrasonic nebulizer injected directly into the torch. The oxy-acetylene flame core reaches temperatures as high as 3000 °C. Unlike other versions of this technology, the flame is not produced by the precursor solvent but by an oxy-acetylene gas mixture. This process has been named oxy-acetylene combustion-assisted aerosol-chemical vapor deposition (OACAACVD).

Researchers at Georgia Tech and nGimat (formerly MicroCoating Technologies) are using the only known commercialized system for combustion chemical vapor deposition (CCVD). The system consists of a proprietary spray/combustion nozzle, the Nanomiser[®], which functions on pressure and heat input for formation of very small droplets that are then combusted by a ring of methane/oxygen pilot light (Ref 77, 78). The solution is delivered under pressure to the nozzle and heated prior to exit.

Steele and Choy at the Imperial College of London have been using a system of deposition named flame-assisted vapor deposition (FAVD). The system was first reported in 1995 and work on SOFC cathode materials was published originally in 1997 (Ref 35, 69). The process consists of an air atomizing nozzle and a separate flame. The air atomizer is directed at a substrate on a hotplate and a separate flame is arranged perpendicular between the substrate and the atomizer. The atomized spray passes through the flame and onto the substrate.

Researchers at ETH Zurich recently published work on the deposition of thin films of $Ce_{0.8}Gd_{0.2}O_{2-\delta}$ (10 mol% Gd_2O_3 doped CeO_2 , 10CGO) by flame spray deposition. In this study, a liquid solution is prepared by mixing suitable precursors and is fed by a syringe pump into the flame. The precursor solution is atomized through a center capillary tube that is surrounded by a dispersion gas, resulting in a fine aerosol. The aerosol is transported by the gasses through the flame and is then deposited on a substrate. Researchers from Korea worked on the aerosol flame deposition (AFD) system to deposit a Ni-YSZ anode (Ref 79). The AFD system consists of a gas delivery unit, a precursor supply unit including a nebulization system, a reactor containing a torch and rotating wafer stage. In the AFD process, a solution precursor was prepared by dissolving the desired precursors into a solvent that is then atomized into micro-sized aerosol by a nebulizer. The flow rate of precursor is controlled by the flow rate of an argon carrier gas. The combustion unit, made from four concentric quartz tubes, creates three ports for source gas and fuel gases for flame. The nebulized aerosol of precursor solution is supplied to the center tube of the torch, while hydrogen, argon shield, and oxygen are supplied through three ports having different diameters producing the laminar flows of mixture gas. The hydrogen dispersion gas was supplied through an annual gap of

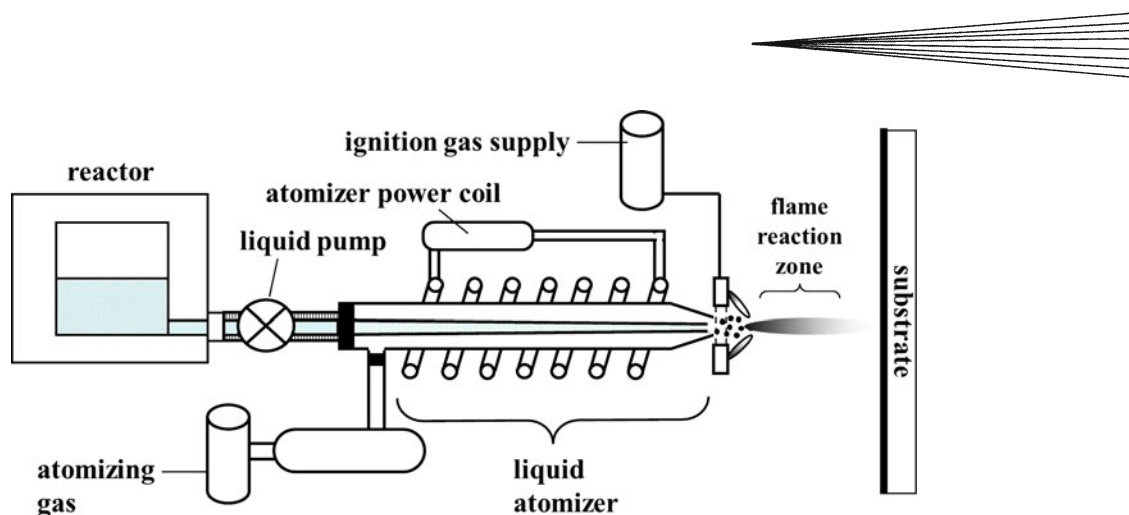


Fig. 2 Schematic of the Reactive Spray Deposition Technique (RSDT) components and liquid delivery system

1.5 mm width having an inner radius of 10 mm from the center of the torch. The precursor solution atomized by a nebulizer was fed into an oxygen-hydrogen flame where the aerosol droplets undergo evaporation, oxidation, and precipitation of particle in the submicron size range. Substrate is heated on a turn-table to prevent the condensation of water on wafer formed during fuel reaction.

The flame deposition process named RSDT was developed by researchers in Canada at the NRC-IFCI (Ref 80, 81). The liquid delivery system comprises off the shelf components from the high performance liquid chromatography (HPLC) and rapid expansion of supercritical spray (RESS) industries for storage and delivery of solutions. A diagram of the process is shown in Fig. 2.

The precursor solution is prepared by dissolving a suitable metal-organic, usually an ethylhexanoate ligand, into a combustible solvent and adding a dissolved gas such as propane. In the process, the liquid feedstock is pumped into a heated tube with at least two decreasing diameters. The temperature of the tube is maintained by an induction coil and the feedback control is a thermocouple placed toward the exit end of the tube. The solution passes through the tube at a process defined pressure and temperature and then exits the nozzle assembly as a very fine spray. A set of pilot igniters comprised oxygen and methane keep the spray combusted as the flame front velocity is too high to be maintained without aid. The flame is then either directed at a suitable substrate for film growth or can alternately be used in a bag-house filter collection system to collect the nanosized particles. Using a heated reactor vessel, RSDT allows the possibility of actually passing a supercritical solution into an atomizer rather than having the atomizer take a solution to the supercritical point in the nozzle prior to exiting as a spray. The off the shelf components for RSDT allow liquid pressures up to 1000 psi and temperatures up to 150 °C prior to introduction into the nozzle. This modification of the process allows the number of solvents and specific precursors used for solution preparation to be increased when compared to other techniques. Nozzle upkeep is easier because fouling in the central tube is eliminated and replacement of the central atomizing tube is less time consuming.

Table 1 RSDT key process parameters and selected range values

| RSDT process parameter | Range of values | Measurement/control |
|----------------------------------|-------------------------------------|---------------------------------|
| Nozzle speed | 5-30 cm/min | Motion controller |
| Flame temperature | 700-1200 °C | Thermocouple |
| Solution concentrations | 10^{-3} to 10^{-1} (mmol) | Premixed by weight |
| Oxygen flow rate | 1-10 L/min | Mass flow controller |
| Atomizer settings | Confidential | Power regulation |
| Precursors for Sm, Ce, Y, and Zr | Ethylhexanoates or acetylacetonates | Solubility in suitable solvents |
| Solvents | Organic | Good solubility of precursors |
| Electrolyte thickness | Will be varied from 50 to 500 nm | Dense |

The deposition configuration for a deposition on an anode-supported SOFC is shown in Fig. 2. For the deposition onto porous substrates, the substrate has to be heated from the back to avoid cracking due to thermal stresses. In the RSDT process, particles are formed by gas to solid particle conversion, whereas in liquid or aerosol flame process this conversion occurs by liquid to solid routes. In the case of liquid to solid conversion and when the droplets are bigger than 1 μm , one particle is derived from one droplet. If the droplet is smaller than 1 μm , as occurs in the RSDT case, when the droplet enters the flame then the solvent will vaporize, followed by precursor decomposition, formation of reactive vapor intermediates, and gas-phase interaction to form particles. Gas to particle conversion refers to production of particles from individual atoms or molecules in the gas phase. The atomization and particle formation processes are understood qualitatively.

The key processing parameters of the RSDT process and some of their range of values are described in Table 1.

2.2 Theory of Operation

Theoretical models describing combustion consider a double-film model for droplet combustion. In this model,

an inner film separates the droplet surface from the flame front, and an outer film separates the flame front from the surrounding oxidizer (Ref 82). The rate of combustion and evaporation is dependent on the size of the generated droplet. As the droplet size decreases, the rate of evaporation of the droplet increases significantly. Therefore, generating smaller droplets in the atomizer can accelerate the combustion rate.

The oxidant/fuel ratio results in different temperature profiles and determines the oxidation strength of the flame. It has been found that higher mixing ratios result in higher maximum temperatures in the flame and lower temperatures at a fixed point at the end of the flame due to shortening of the flame length with increasing oxidant. Eventually, excess oxygen will serve to cool the flame. The temperature profile of the flame affects the chemical reactions occurring and the ratio of products to reactants at a given distance from the nebulizer. Xu et al. (Ref 72) found that crystal orientation was dependant on the oxidant/fuel ratio for YSZ on MgO (1 0 0).

Substrate temperature is another important processing parameter that affects absorption/desorption, reactivity, and diffusivity on the substrate surface. According to the Movchan-Demchishin zone classification on thin film growth, there are three distinct morphological zones. These zones correspond to the ratio of substrate temperature to the melting point of the deposited film (T/T_m). The three zones are as follows (T/T_m): <0.3 , $0.3 < T/T_m < 0.5$, and $0.5 < T/T_m < 1$ (Ref 83). In the zone model, zone I is characterized by low density tapered grains with domed tops. Zone II exhibits more columnar microstructures and the beginning of activation of surface diffusion. Zone III exhibits relatively large equiaxed grains and the activation of bulk diffusion. The model has since been refined to include a transition region (TR) between zones I and II (Ref 84). Polley and Carter (Ref 85) studied the deposition of zinc oxide on amorphous quartz. They found that the nodular growth exhibited in zone I depositions was most likely due to localized shadowing of surrounding nodules. They further speculate that the higher nodules are preferentially deposited on first and deplete the reactants from the gas phase before reaching the underlying regions. This preferential growth means

that atoms do not have sufficient mobility to move to a crystalline site and the films are amorphous. The transition from amorphous to crystalline depositions of zinc oxide on amorphous quartz occurred in the (TR) region. It was further found that increasing the solution concentration from 2.5 to 40 mM shifted the transition temperature from $0.28T_m$ to $0.36 T_m$.

3. SOFC Components by Flame Base Processing

In the proceeding sections, mainly single components of SOFC's made by flame-based process including RSDT were described. The suitability of the different technical approaches must be considered and weighed against their current development maturity. Each approach has to be further examined for suitability of scale up and potential for high volume manufacturing. With this in mind, it is difficult to use the reported performance values as a means of technology assessment, since for this purpose the geometries of each specimen and their respective test parameters, e.g., operating temperature, fuel composition, fuel utilization rate, etc. should be compared in a standardized way (Fig. 3).

3.1 Electrolytes

3.1.1 Electrolyte by Other Flame Processes. Xu investigated deposition of YSZ onto a single crystal Si (1 0 0) substrate. The melting point of YSZ is 2700 °C. According to the Movchan-Demchishin zone classification, zones II and III occur at 810 and 1350 °C, respectively. He found that deposition temperatures of 1230 °C led to films with better faceted crystals and even higher temperatures of 1337 °C led to films with preferred orientation as shown in Fig. 4.

The film growth rate showed two distinct regions with a change in slope of the Arrhenius plot at 1330 °C ($1000/T(K)=0.75$). The lower temperature region has an activation energy of 124.3 kJ/mol and the higher temperature region has an E_a of 19.5 kJ/mol. This indicates a change in the controlling mechanism of film growth from a surface



Fig. 3 Reactive Spray Deposition Setting for SOFC deposition on anode supported cell showing in order the front side deposition, back side heating block and circular mask for deposition

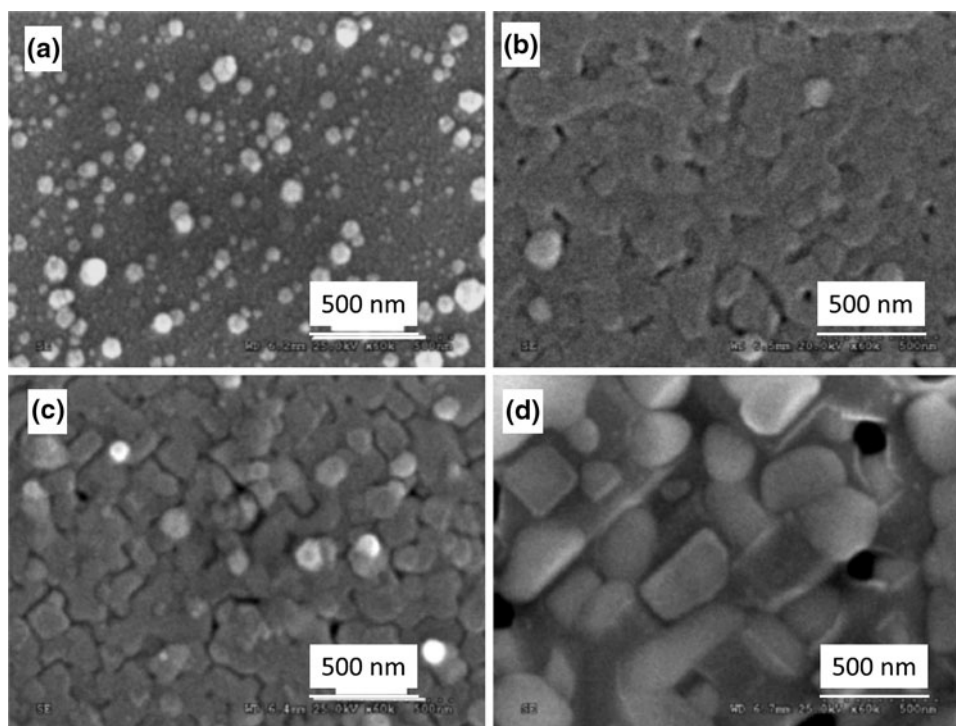


Fig. 4 Deposition of 10 mol% YSZ on Si (1 0 0) single crystal substrate at (a) 945 °C, (b) 1150 °C, (c) 1230 °C, and (d) 1335 °C at a molar flux of 1×10^{-6} mol/min (reprinted from Ref 72 with permission from Elsevier)

reaction controlled mechanism to a gas phase diffusion controlled mechanism as shown by the micrographs in Fig. 4.

Earlier study by Xu et al. (Ref 86) focused on the mechanical properties of composite YSZ- Al_2O_3 electrolytes produced by both PLD and CCVD. He found that films deposited by CCVD had larger grain sizes and surface roughness than PLD-deposited films. It was further found that YSZ was strengthened by addition of alumina. Electrical conductivity was not measured but is expected to improve due to eliminating grain boundary impurities such as SiO_2 and Na_2O via the scavenging effect. The alumina, yttrium, and zirconium were all prepared in toluene from metal acetylacetonates with a total metal concentration of 2.75 mM and deposited at a rate of 2 mL/min (5.5×10^{-6} mol/min) onto a 1200 °C Si (1 0 0) substrate.

Meng and researchers (Ref 70, 71) at the University of Science and Technology of China investigated samarium- and gadolinium-doped ceria via what they termed an oxy-acetylene combustion-assisted aerosol-chemical vapor deposition (OACAACVD) technique. Meng's research group has also focused heavily on research of SOFC materials using aerosol-assisted chemical vapor deposition (AACVD). AACVD is essentially a spray pyrolysis technique followed by introduction of the spray plume into an oxy-acetylene flame. OACAACVD was used to deposit $\text{Ce}_{0.8}\text{Gd}_{0.2}\text{O}_{1.9}$ on poly-crystalline NiO-YSZ, (1 0 0) CeO_2 , and (1 1 1) Si wafers. Solutions of $\text{Ce}(\text{NO})_3$ and $\text{Gd}(\text{NO})_3$ with total metal concentrations of 10 to 50 mM were atomized into the torch at a feed rate of 0.4 mL/min (4×10^{-6} mol/min). The deposition temper-

ature was measured by a thermocouple placed just above the substrate surface. Deposition temperatures of 900–1400 °C were performed. Single-phase GDC with a fluorite cubic structure was obtained with (1 1 1) preferred orientation onto the poly-crystalline NiO-YSZ as shown in Fig. 5.

The melting point of CeO_2 is 2700 °C and three zones with distinct morphologies were identified at precursor concentrations of 10 mM. Zone I ($T_s < 1000$ °C, $T_s/T_m < 0.35$) is characterized by dispersed isolated grains and non-continuous films. Again, this zone indicates a lack of sufficient mobility of the depositing atoms to diffuse over the substrate surface. Zone II ($T_s = 1000$ –1300 °C, $0.35 < T_s/T_m < 0.48$) was characterized by smooth surfaces and uniform columnar grains. Increasing the temperature in zone II resulted in increased density of the film and coalescence of inter-crystalline boundaries. In zone II, the growth rate increased from 0.2 to 0.7 $\mu\text{m}/\text{h}$. Zone III depositions ($T_s > 1300$ °C, $T_s/T_m > 0.48$) consisted of coarse and imperfect surface due to suspected etching by the hyper-thermal flame.

As seen elsewhere, excessive precursor concentration always produced a non-uniform film surface with prominent clusters (~ 0.6 μm in diameter) composed of much smaller grains (~ 0.2 μm in diameter). In Meng's experiments, a 20 mM solution deposited at 1200 °C possessed this type of structure as seen in (e) above. The cauliflower-type morphology is speculated to be a result of secondary nucleation and/or vapor nucleation.

The anode/electrolyte substrate and film deposited at 1200 °C from a 10 mM solution was reduced in H_2 at

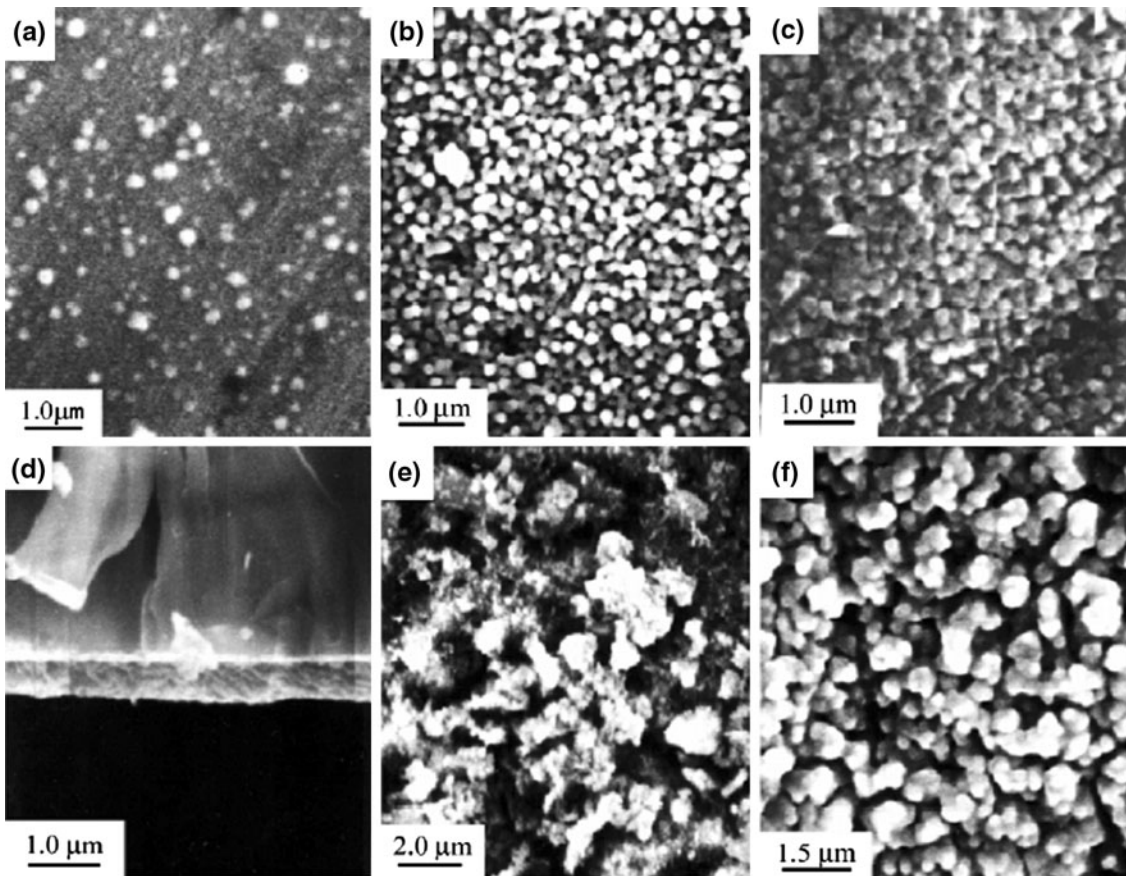


Fig. 5 Deposition of GDC films by OACAACVD onto Ni-YSZ at (a-c) 900-1200 °C, 10 mM (4×10^{-6} mol/min) (d) cross-sectional view 1200 °C, (e) 1400 °C, and (f) 1200 °C, 20 mM (reprinted from Ref 71 with permission from Elsevier)

600 °C and investigated with an AC impedance analyzer in air/Ar. The cell was sandwiched between silver electrodes as follows: Ag/GDC film/Ni-YSZ/Ag.

There are two distinct activation energies for the GDC film in the regions of 350-450 and 450-800 °C that correspond to 106 and 66.5 kJ/mol, respectively, as shown in Fig. 6. At relatively low temperatures, dopant cations and vacancies form neutral defect pairs and the activation energy for conduction is a combination of the binding energy of the associates and the vacancy migration enthalpy. At high temperatures, the conductivity is related to the intrinsic defects, which is dominated by vacancies, known as the “disorder effect” (Ref 87). The ionic conductivity of the grown film was lower than that of sintered GDC material prepared from powder due to a lower than theoretical maximum density of the film (Ref 77). However, the ionic conductivity was higher than that of sintered YSZ. At 600 °C the conductivity was 1.81×10^{-3} S/cm and at 500 °C was 5.15×10^{-4} S/cm, which is rather low.

3.1.2 Electrolyte by RSDT Process. Ni-YSZ anodes with thickness of 300 μm and porosity of 35% have been

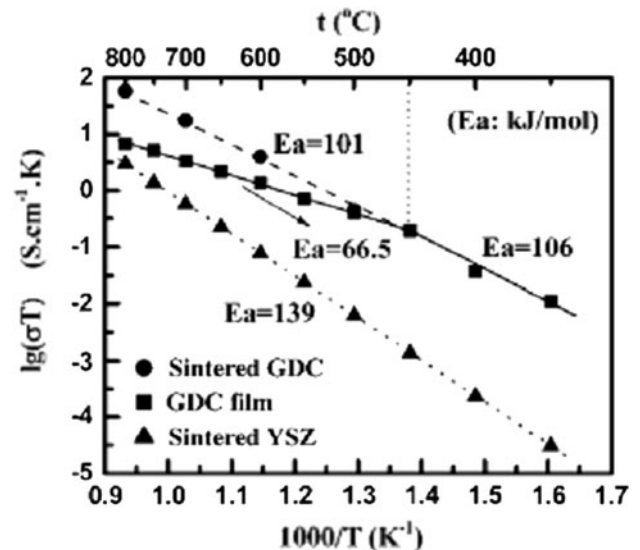


Fig. 6 Arrhenius plots of GDC film deposited on NiO-YSZ at 1200 °C with a 10 mM solution (reprinted from Ref 70 with permission from Elsevier)

used as substrates (supports) for depositing electrolyte layers of 8YSZ (8 mol% Y_2O_3) and GCO (20% at Gd) by the RSDT process. The research was based on understanding the influence of the substrate temperature and process parameters on the deposition rate, nucleation, and growth on dense substrates. For both precursors, metal salts of ethylhexanoic acid dissolved in toluene were used.

Pellets of the anode support were placed into the RSDT furnace and brought to temperatures between 850 and 900 °C with a heating rate of 10°/min. The presence of the deposition flame increased the temperature of the pellet's surface to 950-1050 °C. However, the temperature on the back of the substrate (heater) was maintained constant during deposition. Formation and evolution of coatings was observed while varying process parameters like precursor concentration, deposition (flame) temperature, substrate's temperature and deposition time.

Formation of Layers—Effect of Deposition Time.

Solutions containing 2 mM of precursors have been used to deposit YSZ on anode pellets preheated at 850 °C. The flame temperature at deposition was maintained around 1050 °C, while the average temperature of the substrate was ~1000 °C. Evolution of the coatings' microstructure is shown in Fig. 7. After 15 min of deposition, Fig. 7(a), the surface of the substrate is covered by a very sparse population of crystals. Most of them are small (100-200 nm), few are very large (1-5 μ m), with only some of the crystals being 500 nm to 1 μ m. Surprisingly, there are no crystals in the range of 200-500 nm or below 50 nm.

After 60 min of deposition, Fig. 7(c), large multi-crystalline edifices seem to have grown around the big crystals seen on the 15 min sample. It is important to mention that the longer deposition time, lower concentration, and flow rates were chosen for research purposes to investigate the technically challenging growth of a fully dense electrolyte (99% density) on a 40% porous anode layer. The electrolyte could be deposited for a shorter time by increasing the concentration of material in solution and deposition rate for this research unit. To make the process more suitable for industrial applications multiple nozzles could be utilized and/or the atomization nozzle could be enlarged to accommodate higher flow rates. The original crystals do not seem to have grown any larger after 60 min, but rather served as support for a second population of smaller (within a few hundred nm) crystals that are embedded in the larger crystals in addition to filling the space between them. The size and the density of the small (100-200 nm) crystals do not seem to have increased with time. It is difficult to say if the areas between the large crystals, where the morphology of the substrate is clearly visible, is still not covered or is coated by only a very thin (100-200 nm) layer of YSZ.

After 2 h of deposition, Fig. 7(d), the surface is almost entirely covered by polycrystalline edifices. The areas in between them are smaller and seem to be covered with a thin (probably around 500 nm) nanocrystalline layer containing (embedding) larger 100-300 μ m crystals similar to those originally seen on the 15 min sample. The same type of layer/crystals have grown inside the open pores on

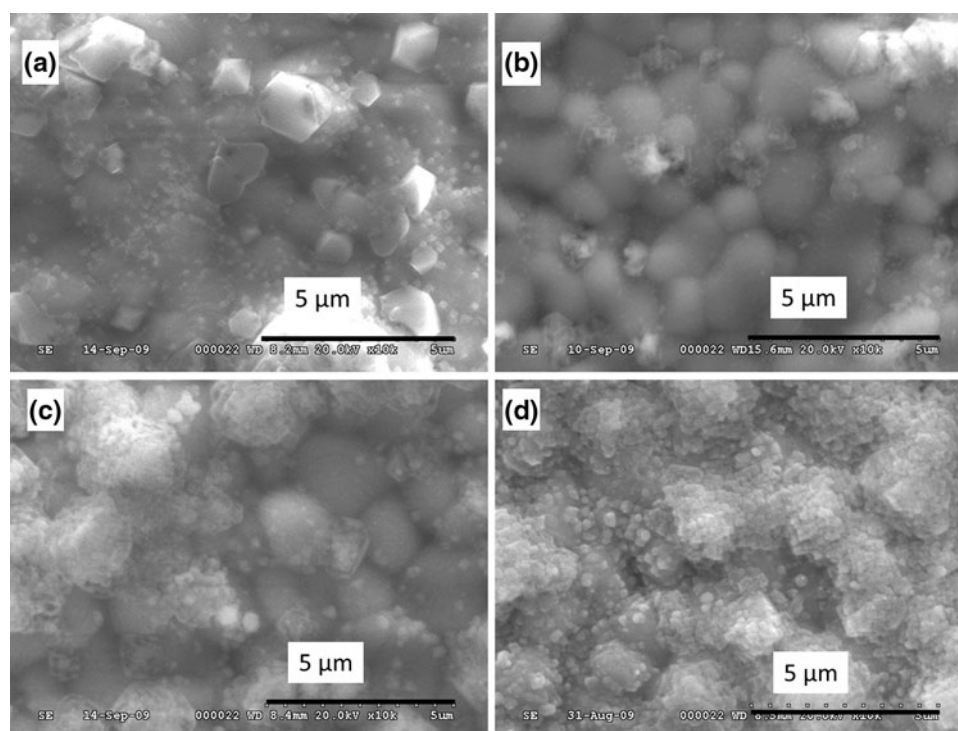


Fig. 7 Morphology of 8YSZ coating on 5 × 5 cm anodes as function of deposition time (a) 15 min, (b) 30 min, (c) 60 min, and (d) 2 h

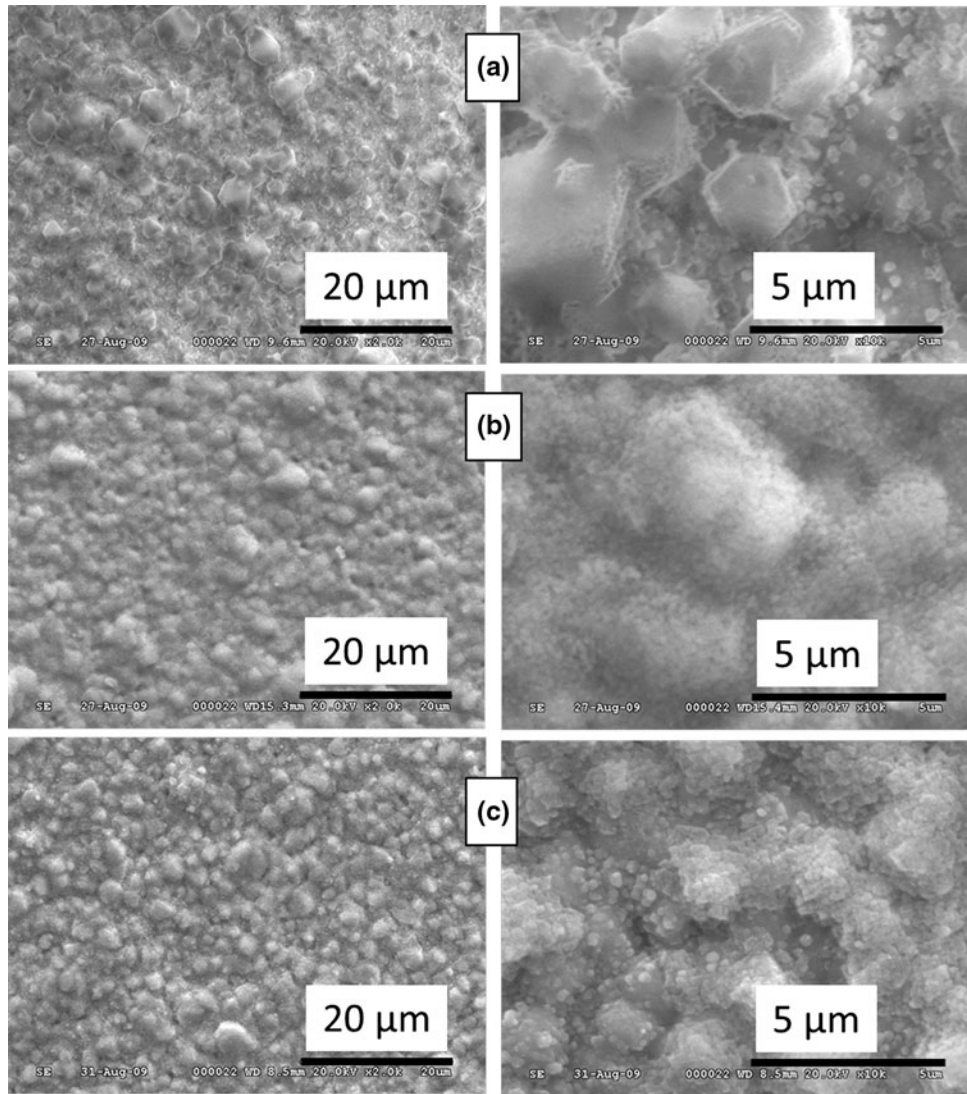


Fig. 8 Evolution of the YSZ coating microstructure on 5×5 cm Ni-YSZ anode supports with precursor concentration (a) 0.5 mM, (b) 1.0 mM, and (c) 2.0 mM

the substrate, clogging them. There is a large variation of the layer's thickness; the polycrystalline edifices are as thick as $3 \mu\text{m}$, while in other areas the coating is less than half a micron thick.

Effect of Precursor's Concentration. The concentration of the precursor solution was changed between 0.5 and 2 mM while the temperature conditions were maintained constant and similar to the previous set of experiments. Coating times were kept constant at 2 h. Evolution of the YSZ microstructure is shown in Fig. 8. The 0.5 mM sample shows a mixture of small, 100-500 nm crystals and large, 2-5 μm polycrystalline edifices with a rather flat aspect. Again, there are little, if any, crystals with other sizes and in the areas not covered by polycrystalline edifices the substrate microstructure is visible, but this time an ultra-thin layer seems to be present over the whole substrate's surface. As the concentration increases to

1 mM, the whole substrate is covered by a continuous polycrystalline layer. The size of the crystals is very uniform and small: 100-200 nm. There are no uncovered areas on the substrate suggesting a thin base layer, although the coating is not flat. Its aspect suggests that those initially separated polycrystalline edifices are, subsequently, covered by a layer of ~ 200 nm crystals.

At 2 mM, the general aspect is similar to that of the 1 mM sample, but both the roughness of the coating and the size of the crystals that form from it are larger. This time the smaller crystals are in the range of 200 to 500 nm (compared to ~ 100 nm at 1 mM). The concentration of the precursor solution seems to shift the layer growth mechanism. Nucleation of growing centers seems to be favored at higher concentration hence the mechanism changes from favoring the preferential growth of large crystals at low concentration to a more homogenous multi-center growth at higher concentration. However, at even

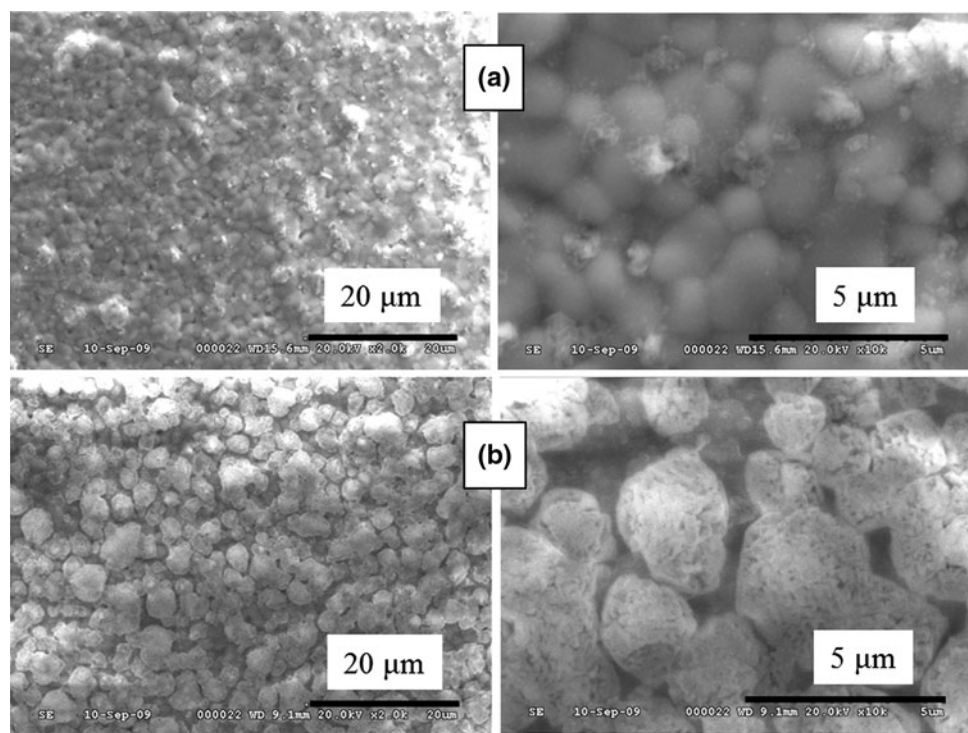


Fig. 9 The effect of the deposition temperature on 5 × 5 cm Ni-YSZ anode supports (a) 950 °C and (b) 1050 °C

higher concentrations the growth is accelerated to such extent that the growth in the direction of concentration gradient is accelerated and larger structures tend to form rough, non-homogenous layers.

Effect of Flame Temperature. Two 30 min coatings, using a 2 mM precursor solution, have been carried on at flame temperatures of ~950 and ~1050 °C. The differences are significant: while the 950 °C sample is covered by an apparently continuous layer of very fine crystals, shown in Fig. 9(a), the 1050 °C sample, Fig. 9(b), exhibits a totally different microstructure, with very large (~5 μm) polycrystalline structures growing above the substrate. It is not clear why there is such a clear segregation between the sizes of the crystals that occur during the first stages of the layer formation. Once this segregation occurs, it seems to take control over the growth of the layer. Further studies are currently in progress to better understand correlation between the concentration and the chemistry of the coating and the interaction of the growth with the substrate composition. In our opinion, this initial growth phase is critical in determining the subsequent growth rate, mechanism, and final microstructure (i.e., density) of the coating.

Although our previous experience with other ceramic materials, in particular SOFC cathodes, as well as literature in the data seemed to suggest that a higher temperature in the deposition zone will favor a dense microstructure, present results contradict this hypothesis. An extremely fast preferential growth seems to occur, suggesting that the higher temperature gradient in the

direction of the layer's growth generated by the higher flame temperature favors the preferential growth over the surface diffusion and nucleation.

Effect of Solution Chemistry. In the next investigation the solvent was switched to ethanol and the solutes were switched to $Zr(CH_3(CH_2)_3CH(C_2H_5)CO_2H)_4$ and $Y(NO_3)_3$ for 8YSZ ceramic film preparation. Continuous layers of YSZ ~2 μm thick were successfully deposited on porous NiO-YSZ composite pellets as shown by the micrographs in Fig. 10. The layers exhibit a rough microstructure, with large crystal-like features as shown in Fig. 10(b), after 1 h of deposition. The coating manages to cover most of the substrate's pores as shown in Fig. 10(b) when compared to Fig. 10(a) (5 min of deposition). A cross section of the layer is shown in Fig. 10(c).

The coating seems to form by coalescence of individual growth centers. The growth of these centers is faster perpendicular to the surface of the substrate. On a rough substrate some areas have more growing centers than others and some of these centers grow faster. Our first investigations show that the layer has a porous base as individual centers form and start growing and a dense top as these growing columns coalesce further from the substrate. A possible solution is a two-step deposition process, the first step being run with very low precursor concentration to favor the formation of a dense base layer. However, this effect is strongly dependent on the roughness of the substrate and formation of a dense layer on a porous substrate is a challenging endeavor. A porous and rough substrate would normally enhance the effect, but in

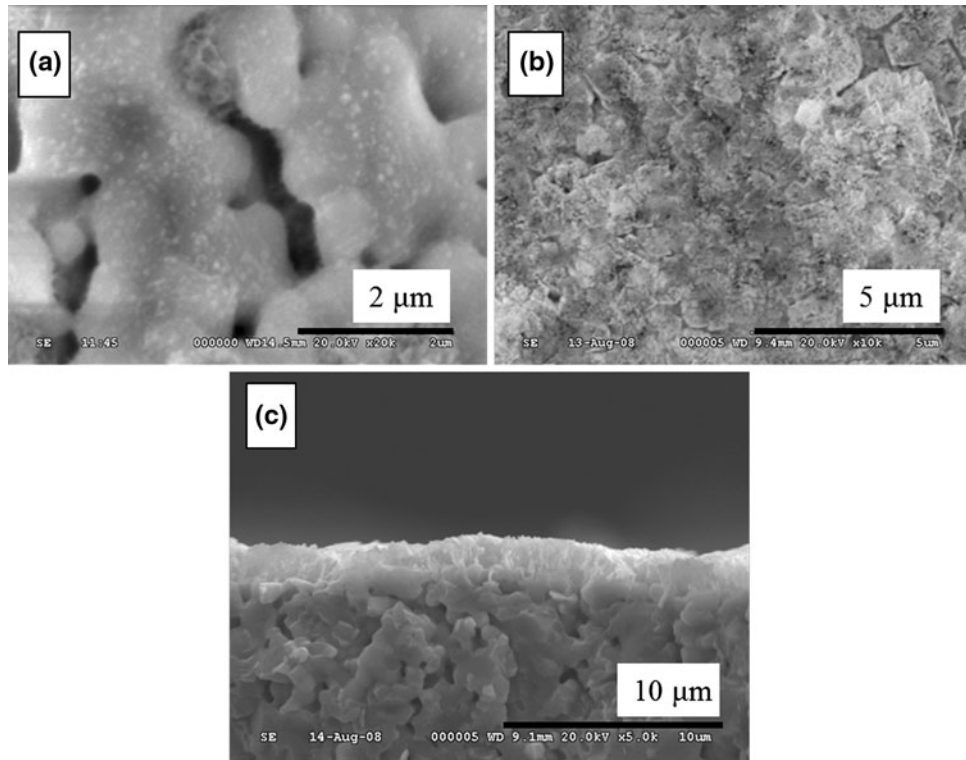


Fig. 10 8YSZ coatings onto porous 5 × 5 cm Ni-YSZ anode supports (a) 5 min, (b) 60 min, (c) cross section of 60 min coating

such a case the initial porosity of the electrolyte layer would be smaller than the substrate porosity and would act like a graded passage from electrode's microstructure to the dense electrolyte. On a more dense and flat substrate the growth mechanism would lead to less porous, eventually dense layers. This statement is supported by investigations on gadolinium-doped ceria (GDC) coatings deposited on dense YSZ electrolyte substrates as blocking layers which are discussed in the following section. These coatings were fully dense, with no base porosity. Work continues on further understanding and optimization of the process, on reducing the initial porosity and evaluation of structural and electrochemical properties on both standard and real anode substrates.

3.2 Cathodes

3.2.1 Cathode by Other Flame Processes. Liu et al. (Ref 88) found that deposition temperature has a significant impact on cathode morphology as well as interfacial resistance. Interfacial resistance was reduced from 24.8 to 0.26 $\Omega \text{ cm}^2$ by increasing the deposition temperature from 800 to 1400 °C as shown in Fig. 11. Deposition temperatures less than 1000 °C resulted in high interfacial resistances while temperatures above 1400 °C resulted in cathodes that were too dense. Composite electrodes of 70 wt.% $\text{Sm}_{0.5}\text{Sr}_{0.5}\text{CoO}_{3-\delta}$ and 30% $\text{Sm}_{0.1}\text{Ce}_{0.9}\text{O}_{2-\delta}$ were deposited on a 10% Gd-doped ceria pressed pellet 10 mm in diameter (see the SEM images in Fig. 12). Undesirable densification occurred at 1400 °C. This densification would undesirably impede gas flow. Deposition flow rates of

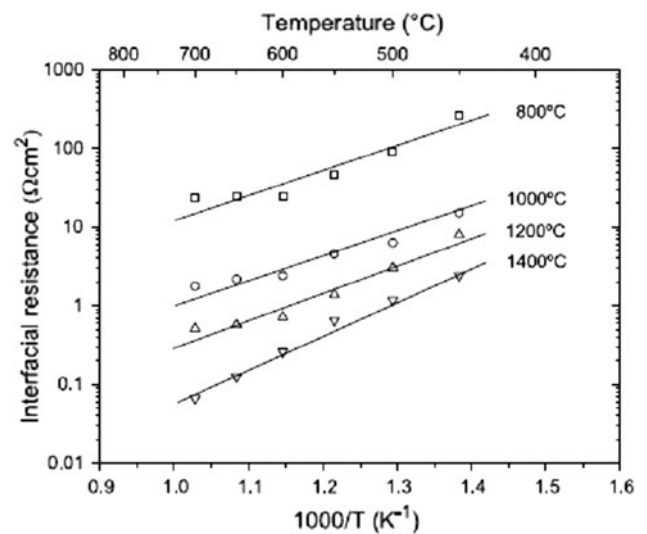


Fig. 11 Interfacial polarization resistances of symmetrical cells determined from impedance spectroscopy (Reprinted from Ref 88 with permission from Elsevier)

4-6.5 mL/min were common for the process. Solution concentrations from 5 to 250 mM were investigated and it was found that the morphology was similar for a given solute flux but that lower concentrations showed better performance presumably due to longer deposition dwell times that caused better particle to particle contact and particle to substrate adhesion.

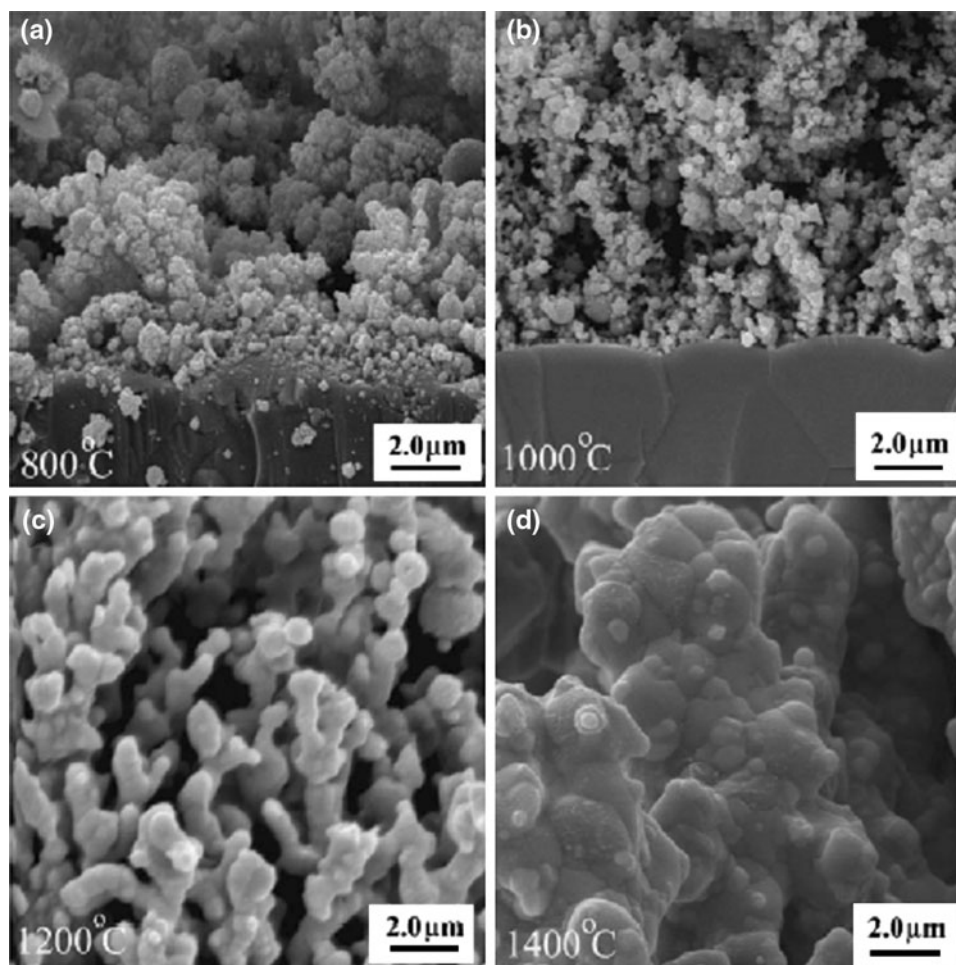


Fig. 12 Deposition of 70 wt.% $\text{Sm}_{0.5}\text{Sr}_{0.5}\text{CoO}_{3-\delta}$ and 30% $\text{Sm}_{0.1}\text{Ce}_{0.9}\text{O}_{2-\delta}$ cathodes onto 10% Gd-doped ceria pressed powder pellets at 800-1400 °C (1.5×10^{-4} mol/min) (reprinted from Ref 88 with permission from Elsevier)

Steele and co-workers (Ref 35) at the Imperial College of London deposited $\text{La}_{1-x}\text{Sr}_x\text{MnO}_3$ (LSM) onto 10 mm diameter, 0.5-0.7 mm thick 8 mol% YSZ pellets pressed and sintered in air at 1500 °C for 2 h (density > 98%). Precursor solutions consisted of metal nitrates at concentrations of 10-100 mM in ethanol/water mixtures. The following process parameters were examined in the article: ethanol/water ratio of the precursor solution, flow rate, precursor concentration, atomizer pressure, and nozzle to substrate distance.

The ethanol/water ratio of the precursor solution was varied from 80/20 to 60/40. It was determined that ratios of 80/20 ethanol/water (50 mM concentration and 12 mL/min) at a precursor flux of 6×10^{-4} mol/min produced poorly adhering powdery agglomerates less than 1 μm in diameter. At ethanol/water ratios of 70/30 the film was a uniform porous film of large particles (10-20 μm). At 60/40 ethanol/water the film was nearly dense with a few large particles. XRD spectra of the as deposited films indicate that at 60/40 the fuel was not sufficient to combust all the droplets and some un-combusted droplets splashed onto the heated substrate leaving a flaky amorphous film. At medium ratios of 70/30, heterogeneous nucleation

occurred near the vicinity of the substrate resulting in a dense film. The XRD spectra show the crystalline peaks of LSM for ratios equal to and higher than 70/30.

The effect of flow rates from 5.5 to 17 mL/min was examined using 50 mM 80/20 solutions (2.75×10^{-4} to 8.5×10^{-4} mol/min). The film produced at 5.5 mL/min was much denser than the powdery films produced at 17 mL/min. The microstructure of the low flow rate indicates that the combustion and decomposition reactions occurred in the gas phase. XRD data indicate that the powdery layer was more crystalline than the film deposited at 17 mL/min. SEM images indicate that un-combusted droplets penetrated the flame at the high flow rates to form a dense and eventually cracked film with little crystallinity.

The effect of solution concentration from 50 to 100 mM was studied with a 70/30 solution at 12 mL/min (6×10^{-4} to 1.2×10^{-3} mol/min). The SEM images show that the size of the particles is largest at high concentrations (100 mM) and smallest at low concentration (10 mM). In addition, agglomeration was also highest for more concentrated solutions. The porosity of the films is highest when formed from large particle sizes and a high degree of

agglomeration. The films show less agglomeration at reduced concentration. At low concentration, particles are farther apart and have less probability of encountering another particle and agglomerating. Similar concentration influences have been reported by Messing using a spray pyrolysis technique (Ref 89).

Finally, Steele et al. studied air atomizer pressure between 17 and 30 psi on a 50 mM 70/30 solution at 12 mL/min (6×10^{-4} mol/min). At low pressures (17 psi) the film was powdery with fine particle sizes, smaller than $2 \mu\text{m}$ ($T_s = 720\text{--}770 \text{ }^\circ\text{C}$). Raising the pressure to 22 psi lowered sample temperature to $680\text{--}730 \text{ }^\circ\text{C}$. Further increasing the pressure to 26 psi resulted in more densely packed and larger particles up to $20 \mu\text{m}$ with some cracks. The higher pressure resulted in further cooling of the substrate temperature to $450\text{--}500 \text{ }^\circ\text{C}$. XRD spectra show that the powdery films deposited at lower pressure show larger substrate peaks while the films deposited below 22 psi show a marked decrease in substrate peaks.

Karageorgakis et al. at the ETH Zurich deposited $\text{La}_{0.6}\text{Sr}_{0.4}\text{CoO}_{3-\delta}$ (LSC) with dense and crack-free microstructures. The surface of the film is particle-free, unlike films from other flame-based deposition techniques, such as CCVD and AACVD (Ref 35). The LSC films were deposited for 10 min symmetrically on CGO pellets with dimension of $1 \times 1 \text{ cm}$.

3.2.2 Depositions— $\text{Sm}_{0.5}\text{Sr}_{0.5}\text{CoO}_3$ (SSCo) Cathodes: By RSDT Process. SSSCo cathode material layers have been successfully deposited onto anode-supported cells containing SDC electrolytes. Both phase and chemical composition of the layers have shown to be consistent with a fully crystalline SSSCo ceramic (Ref 49). We have been able to modify their microstructure, in a controllable manner, from dense and fairly flat to porous and columnar. Both concentration and substrate temperature can be used as independent process parameters to control the evolution of the microstructure as shown in Fig. 13 and 14.

SSCo cathode layers with identical microstructures have been deposited under physically identical conditions with precursor feeds of similar concentrations, but using toluene or ethanol as the solvent. Sm-nitrate, Sr 2-ethylhexanoate, and Co-acetate were used as precursor salts in ethanol-based solutions. Depositions of SSSCo cathodes were done on half-cell substrates (SDC electrolyte) made by NRC-IFCI. A typical microstructure is shown in Fig. 15, while Fig. 16 shows an EDX spectrum of the same coating. The coatings exhibit a porous columnar

microstructure $2\text{--}3 \mu\text{m}$ high. Previous test results (on NiO-YSZ/NiO-SDC/SDC button cells coated using toluene-based solutions) have shown a 35% increase on the peak power density and $\sim 25\%$ decrease of the polarization resistance compared to screen printed cathodes of similar composition.

Testing of SOFC button cells with SSSCo cathodes made by RSDT, against reference cells of the same size with screen printed SSSCo cathodes, have shown a remarkable 34% increase in peak power density (PPD) and a significant 20% decrease in total polarization resistance at $600 \text{ }^\circ\text{C}$ (R_p , Table 2) (Ref 11).

The porosity of the cathode is important for the supply of oxygen to the triple phase boundaries (TPB), which can occur via O_2 molecules moving through pores in the cathode layer, or via adsorbed O-atoms in a surface diffusion process. The RSDT cathode has more open pores, compared to the more closed pore structure of the screen printed and sintered cathode which allow gas to easier diffuse to the interface between the cathode and the electrolyte where the TPBs are concentrated, and that leads to better electrochemical properties of the RSDT cathode. However, the size of pores has to be optimized as a too large a porosity could have a detrimental effect on the electrical conductivity of the cathode. The large inter-grain contact at the interface of the electrode/electrolyte favors the electrochemical oxygen reduction reaction.

3.3 Deposition of Diffusion Blocking Layers by RSDT Process

The composition of (La, Sr)-manganites (LSM) has a strong influence on the chemical reaction between the cathode and the electrolyte. A very important factor for the long-term stability of the SOFCs is that no highly resistive phases are formed due to reaction between these two materials. Two phases $\text{La}_2\text{Zr}_2\text{O}_7$ and SrZrO_3 may form at the cathode/electrolyte interface either during fabrication (sintering at $1100\text{--}1400 \text{ }^\circ\text{C}$) or during long-term operation. The formation of La and Sr-zirconates has a detrimental effect on the performance of the SOFC by blocking the TPBs because of their high resistivity.

In order to prevent the solid state reaction of YSZ electrolytes and Sr containing cathode materials during normal functioning of SOFC at temperatures around $700 \text{ }^\circ\text{C}$, an inter-layer of ceria-based electrolytes is usually deposited at the YSZ-cathode interface (Ref 26).

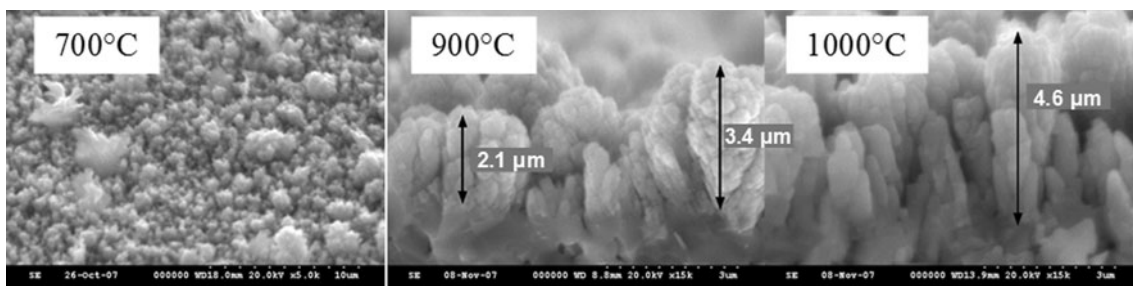


Fig. 13 Evolution of SSSCo microstructure with the substrate temperature (a) $700 \text{ }^\circ\text{C}$, (b) $900 \text{ }^\circ\text{C}$, and (c) $1000 \text{ }^\circ\text{C}$

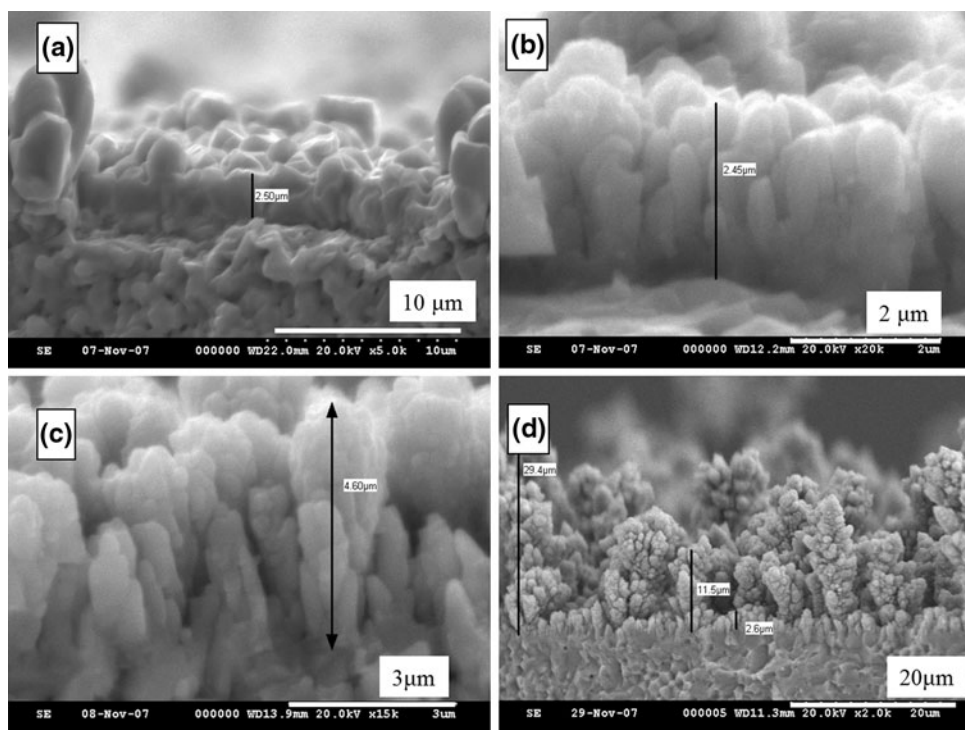


Fig. 14 Evolution of SSCO microstructure with the precursors' concentration (a) 0.85 mM, (b) 2.3 mM, (c) 4.6 mM, and (d) 9.2 mM

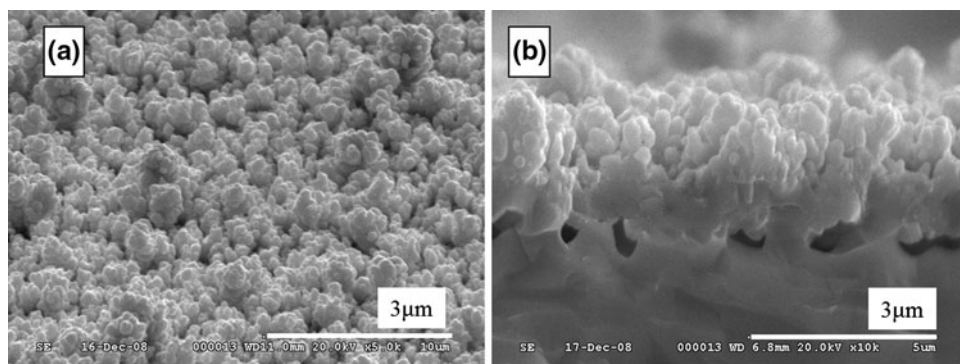


Fig. 15 SEM images of SSCO cathode coating on half cell substrate (a) surface (b) cross section

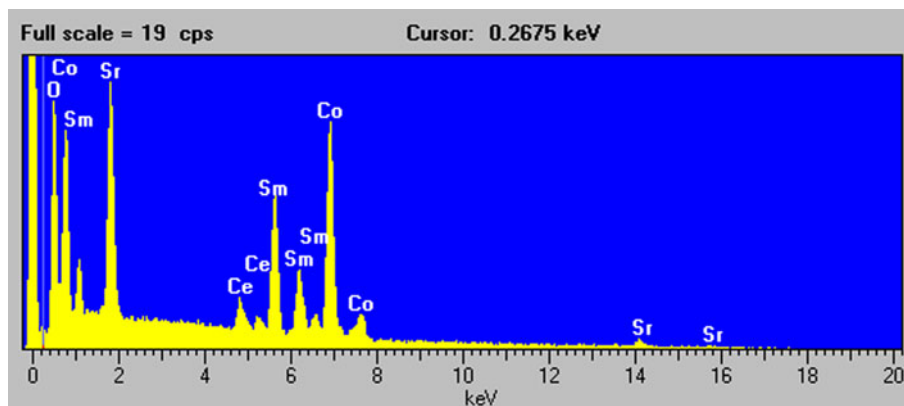


Fig. 16 EDX spectrum of the SSCO coating shown in Fig. 15

Cerium-gadolinium oxide with the generic formula $Ce_{0.8}Gd_{0.2}O_{2-\delta}$ has been deposited on top of a YSZ electrolyte by RSDT to examine this blocking behavior.

To obtain CGO layers with different thicknesses, deposition times between 30 and 240 min were used while

Table 2 Comparison of electrochemical performance data of SSCO cathodes applied by a screen printing method and the RSDT method

| Cell parameter | Cathode processing | |
|---|--------------------|-------|
| | Screen printed | RSDT |
| OCV, V | 0.812 | 0.84 |
| R_s , Ω cm ² | 0.129 | 0.120 |
| R_p ($a+c$), Ω cm ² | 0.102 | 0.079 |
| PPD, W/cm ² | 0.485 | 0.651 |
| Thickness, μ m | 25 | 20 |

maintaining a constant concentration in the solution. Two substrate temperatures were used at 925 and 1050 °C. While the deposition rate was higher for the higher substrate temperature, the final samples have been prepared below 950 °C to prevent any possible reaction between the CGO layers and substrates. Figure 17 shows SEM images of the top CGO layers after 240, 120, and 60 min on a cell 5 × 5 cm cell. Figure 18 shows the effect of deposition temperature. Again, this long deposition time was chosen for research purposes to make dense pinhole free layers. The blocking layer could potentially be deposited for a shorter time by increasing the solute concentration and/or the flow rate of the solution.

Coatings are continuous and homogeneous; following the underlying microstructure of the electrolyte layer. At longer deposition times, Fig. 17(c), the formation of nanocrystalline edifices and beginning of evolution of small growing centers is observed. The estimated thick-

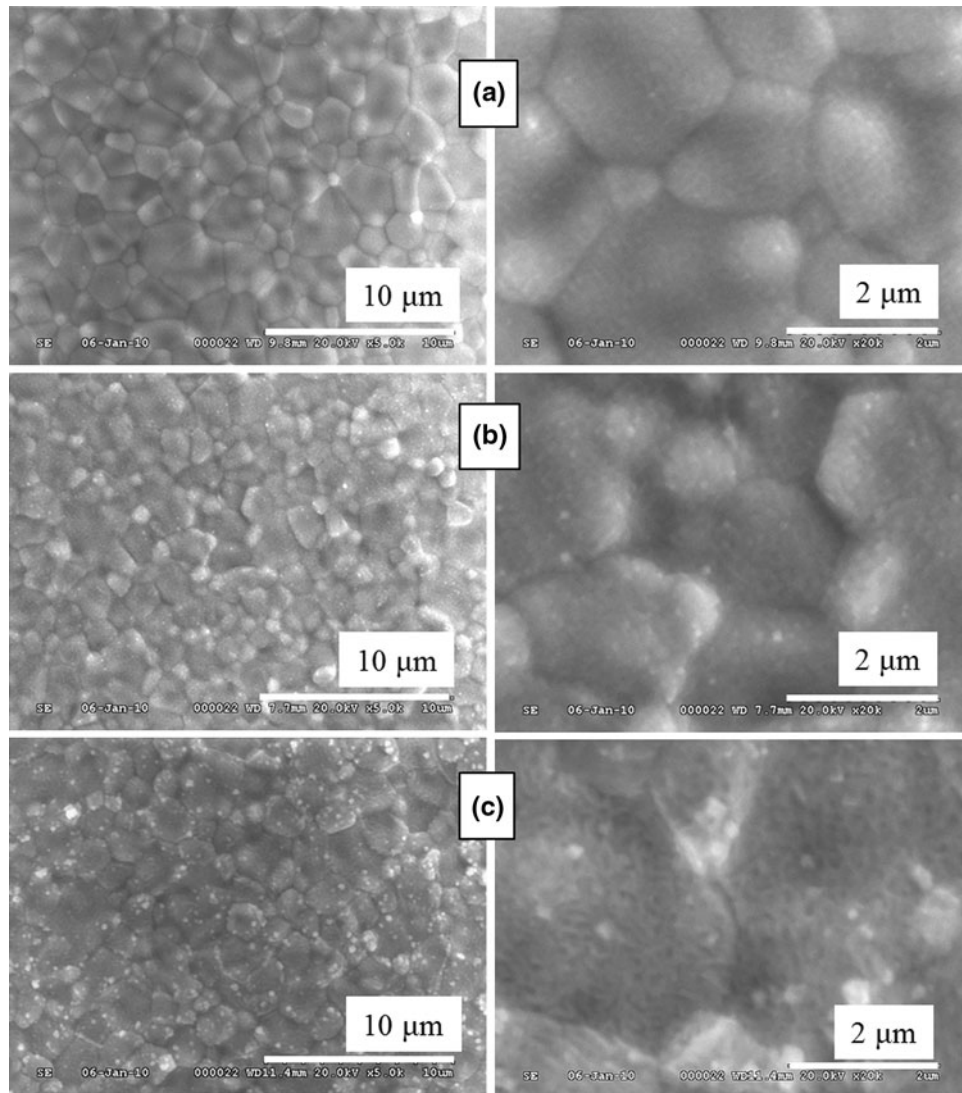


Fig. 17 Microstructure of CGO layers deposited on half-cell substrates at various deposition times. (a) 60 min, (b) 120 min, and (c) 240 min

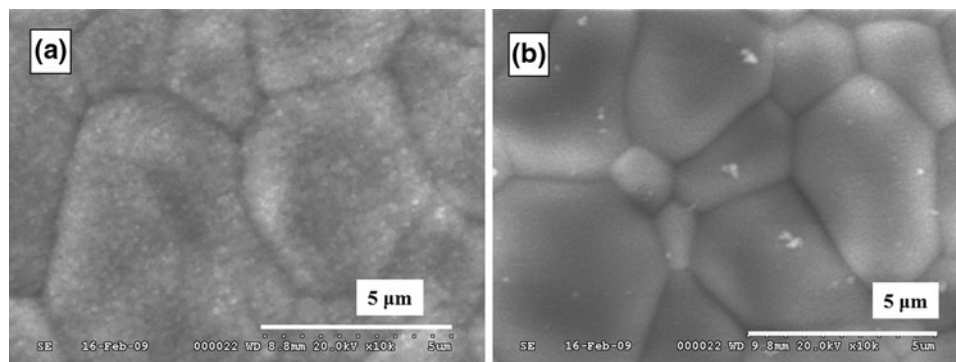


Fig. 18 Top view of GCO coatings on half-cell substrates (a) average deposition temperature 1050 °C, and (b) average deposition temperature 900 °C

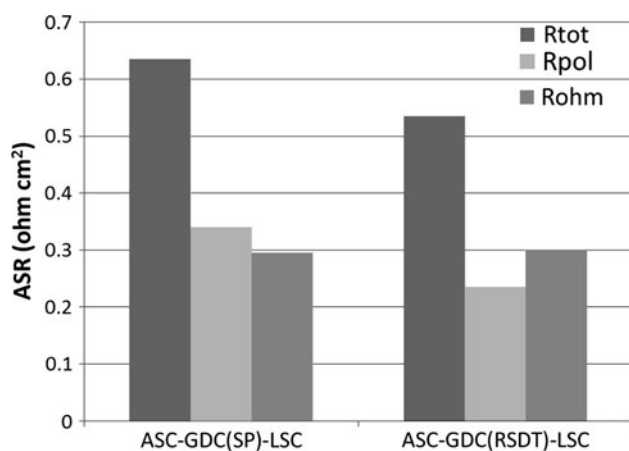


Fig. 19 Total area specific resistance (R_{tot}), ohmic losses (R_{ohm}), and electrode polarization losses (R_{pol}) are given for each cell configuration in Ωcm^2

ness of the CGO layers was between ~ 200 nm for the 30 min depositions and ~ 1.5 μm for the 240 min depositions. Phase composition of the CGO layers was investigated on as-coated substrates by x-ray diffraction and clearly shows the presence of a crystallized cubic CGO phase (Ref 90).

The cells were tested using a screen printed LSC cathode fired at 1000 °C. The tests were conducted under air-hydrogen 3% RH. Similar cells having a CGO layer made by spray pyrolysis (SP) were used as the reference. The performance of the cell having an RSDT made ceria layer is almost double when compared to the cell having a spray pyrolysis made CGO layer (656 mW/cm^2 compared to 360 mW/cm^2) at an operating temperature of 600 °C as shown in Table 2. The thickness of the RSDT blocking layer is 500 nm while the screen printed one is 1 μm . The screen printing process was unable to print a pin-hole free layer less than 1 μm in thickness, while the RSDT process is ideally suited to thinner pin-hole free layers.

The implementation of the ceria barrier layer using RSDT in the anode-supported cell leads to lower ohmic losses, compared to a screen printed GDC layer. The results are summarized in Fig. 19. The thickness of the

blocking layer plays an important role and it has to be optimized to get the lowest ASR without compromising the blocking function of this layer.

A more detailed description of the cell performance improvement in terms of IV-curves and area specific resistance values (ASR) are presented in reference by Maric et al. (Ref 11). The electrochemical performance of anode-supported cells has been further enhanced by optimizing the quality of the ceria-based diffusion barrier to fulfill two requirements for the ceria layer. First, this layer has to be dense to prevent any reactivity between LSC and zirconia electrolyte and formation of $La_2Zr_2O_7$ phases at the standard La-cathode/YSZ interface (Ref 91). Second, this ceria layer needs to be deposited at lower processing temperatures to avoid inter-diffusion of cations between the ceria and zirconia electrolyte that creates a reaction zone with a lower ionic conductivity, leading to increased ohmic losses (Ref 92).

By increasing the operation temperature to 700 °C both ohmic losses and polarization losses decrease. These area specific resistance at 700 °C have been obtained from impedance measurements at a current density of 0.4 A/cm^2 at 600 °C with humidified H_2 (500 mL/min) supplied to anode and synthetic air (400 mL/min O_2 and 1600 mL/min N_2) supplied to the cathode. For two different thicknesses of GDC blocking layers at 200 and 400 nm the ohmic resistance is 0.108 and 0.103 Ωcm^2 , respectively, as shown in Fig. 20. This result shows that once you have a dense layer the blocking layer can be quite thin. When very thin layers are used as diffusion barriers, their microstructural properties must be tuned very precisely. Also, care must be taken to avoid typical defects like pinholes or cracks. Further research on the stability of this type of the cell has to be reviewed.

3.4 Deposition onto Metal Cell Supports

3.4.1 Deposition on Zinc-Coated Steel. Schinking et al. from Thyssen Krup Stahl in conjunction with SurA Plasma investigated the deposition of SiO_2 from tetraethyloxysilane (TEOS) and tetramethylsilane (TMS) onto zinc and polished galvanized steel via a combustion CVD process (Ref 93). SiO_2 is an insulator and was developed to

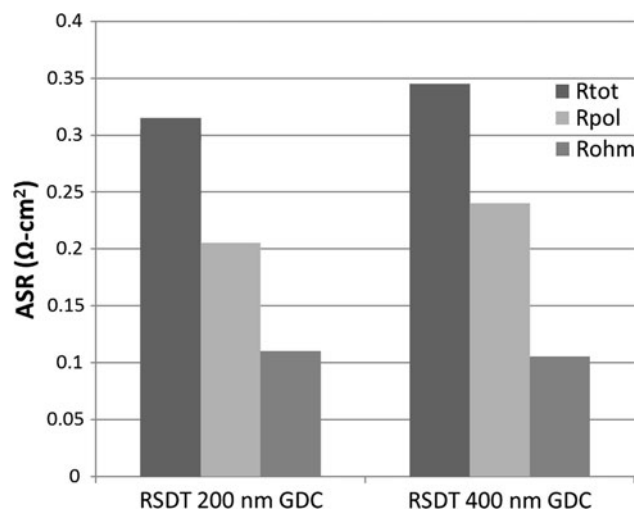


Fig. 20 Total area specific resistance (R_{tot}), ohmic losses (R_{ohm}), electrode polarization losses (R_{pol}) are given for each cell configuration in $\Omega \text{ cm}^2$. These area specific resistance values have been obtained from impedance measurements at a current density of 0.4 A cm^{-2} at 700°C with humidified H_2 (500 mL/min) supplied to anode and synthetic air (400 mL/min O_2 and 1600 mL/min N_2) supplied to cathode

enable wetting and adhesive bonding of metallic and polymeric substrates. The coverage of SiO_2 was determined by cyclic voltammetry. The decrease in oxidation and reduction peaks at -0.8 and -0.97 V (SHE) are monitored as a function of deposition time. While SiO_2 is an insulator and therefore useless as a coating on an interconnect material, it does show that combustion CVD can be used for direct deposition onto metallic supports. Furthermore, XPS and FT-IRRAS analyses showed no increase in the natural oxide thickness of the galvanized steel when the surface was exposed to the deposition flame for the brief periods used in these SiO_2 depositions (Ref 94). This research is interesting since SOFC interconnects made of steel are actively being developed for LT and IT-SOFC applications. Another interesting note is that Tiller has been using flame-based deposition techniques since 1989 (Ref 95, 96).

One way to improve the mechanical properties of solid oxide fuel cells is the development of metal supported designs. It should however be emphasized that the processes involved in fabrication of metal supported SOFC structures should not exceed 1000°C , which is the standard annealing temperature of ferritic stainless steel alloys. The advantages of using metal-supported SOFC might also lead to a considerable reduction of the production costs for such systems. The advantages might also lead to a considerable reduction of the production costs for such systems. However, one persistent problem needs to be solved: Inter-diffusion of chemical elements contained in the metal substrates, especially chromium. In order to address the issues of sintering and delamination for metal-supported SOFC, a deposition of Gadolinia-doped Ceria (GDC) on metal substrates made of Crofer 22 APU was investigated by RSDT. Since metal-supported fuel cells aim at low/intermediate operating temperatures, reducing the thickness of these protective

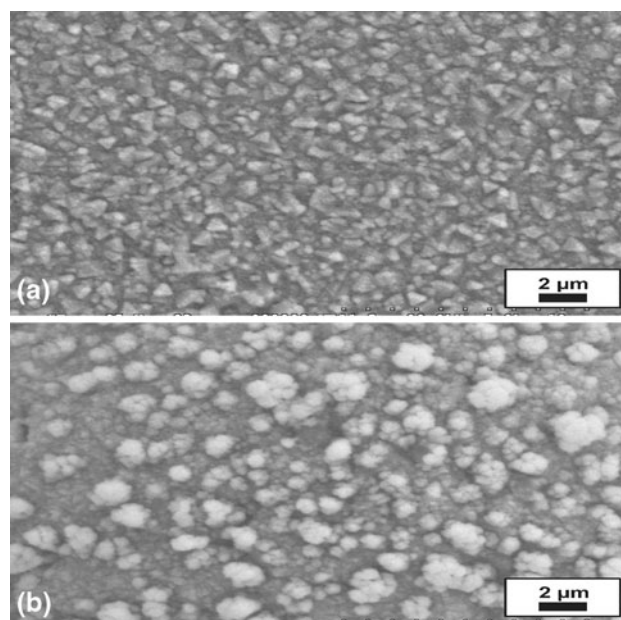


Fig. 21 SEM images of GDC layer deposited using RSDT at a substrate temperature of 800°C . The coating on a flat surface is shown in (a) and the coating on the surface of a porous sample is shown in (b)

coatings is crucial, since layer thickness is directly correlated to its ohmic resistance. During the RSDT deposition, substrate temperature was kept constant at 800°C and a precursor solution concentration of 1.0 mmol/L was used during processing (240 min).

SEM images of the GDC layers deposited by RSDT are shown in Fig. 21. The RSDT particle size lies between 0.5 and $1 \mu\text{m}$. The pyramidal structure of the particles is typical for an initial island growth mechanism. Although identical deposition conditions were used, the result for porous substrates, Fig. 21(b), is totally different from that of dense substrates, Fig. 21(a). Cauliflower-like structures can be seen on the surface of the porous substrate. Hence, this effect is linked to differences in the condensation process of the hot vapors onto plain and porous substrate materials when working in ambient air.

4. Cost of RSDT Processing

The RSDT process and material inputs have been analyzed and compared to the co-firing and multi-firing process outlined in the 2004 TIAX report for an SDC electrolyte layer (Ref 97). The SECA program has outlined target factory costs of $\$400/\text{kW}$ by 2010 as a goal for various commercial products targeted toward residential and industrial combined heat and power units. An earlier 1999 report estimated a low temperature (800°C) compared to a high temperature (1000°C) planar ceramic design of $\$86/\text{kW}$ ($\$430/\text{m}^2$ @ 500 mW/cm^2) using YSZ as the electrolyte. Cost analysis for the TIAX report was performed for the YSZ layer at a nominal thickness of

Table 3 Cost analysis by TIAX broken down by SOFC component layer and two separate processes for a YSZ layer at a nominal thickness of 10 μm

| Co-fire | \$/m ² | | | |
|--------------|-------------------|----------------------|---------------------|----------------------|
| | Material | Process | Multi-fire material | Process |
| Anode | 123.95 | 9.63 | 125.92 | 9.69 |
| Cathode | 18.22 | 7.4 | 14.57 | 7.07 |
| Electrolyte | <i>6.01</i> | <i>6.18</i> | <i>6.11</i> | <i>6.21</i> |
| Interconnect | 118.7 | 19.25 | 118.7 | 19.25 |
| Fabrication | | 100.99 | | 126.72 |
| sub-Total | 266.88 | 143.45 | 265.3 | 168.94 |
| Total | 410.33 | (\$/m ²) | 434.24 | (\$/m ²) |

10 μm . The co-fired process offered the potential of eliminating a sintering step but does not allow tailoring of the sinter temperatures for each layer. A key substitution made in the 2003 cost analysis versus the 1999 analysis was the use of screen printing rather than plasma spray for the formation of the electrolyte layer “due to the difficulty in achieving dense pinhole-free plasma coatings.” The deposition of a dense pin-hole free coating on a porous substrate represents a challenge to any vapor phase deposition process. The Tiax report finds a bulk cost of \$55/kg of 8 mol% YSZ whereas we are using a cost of \$500 for SDC, we are aware that costs could be much higher in the range of \$1500/kg. The report found that by far the dominant factor in power output was the electrolyte thickness due to the ionic resistance.

The factory cost of the electrolyte is broken down into material and process costs. They are listed in Table 3 with the relevant layer highlighted in italics. While the electrolyte layer accounts for only 2% of the material cost and 4% of the total cost it has the capacity to significantly influence the power density and thus reduce cost by cutting down on the required active area. A sensitivity chart in the 2004 TIAX report shows anode layer thickness and electrolyte layer thickness as the two input variables with the largest effect on cost (\$/kW). The cost of the YSZ comes in at a close fourth. A Monte Carlo simulation based on various cost elements has an 87% certainty of the cost being between \$80/kW and \$120/kW. A breakdown of the electrolyte layer is between \$1.27-1.30 \$/kW (materials) and \$1.31-1.32 \$/kW (process).

Cost targets as stated above are quite stringent and performance will dominate the cost balance. Our rough cost breakdown for the RSDT process and inputs has been performed for a 5 μm thick electrolyte layer deposited via lab prices/quantities, in Fig. 22, and bulk process, in Fig. 23, for an SDC electrolyte using a single RSDT processing device with a precursor mass flux of 5.6 mg/min.

Generation of a dense layer may put constraints on the upper flux of material which can be modified by both concentration flow rate as reported earlier in this article. The numbers shown in Table 4 represent levels used in initial lab experiments. Efficiency values of 75 and 100%, in the left and right column respectively, are included as references, however, the exact efficiency will vary depending on chosen deposition conditions. It is expected

RSDT SmCeO electrolyte material + process deposition costs for lab scale @ 75% efficiency for a 5 X 5 cell

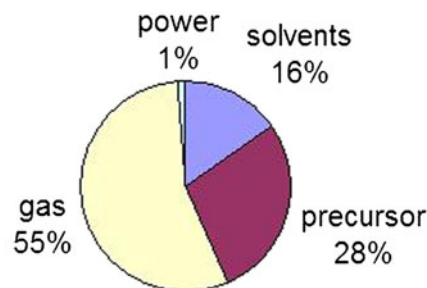


Fig. 22 Lab scale process costs of RSDT for a 5 \times 5 cell at 75% efficiency

RSDT SmCeO electrolyte deposition costs for bulk scale @ 75% efficiency for a 5 X 5 cell

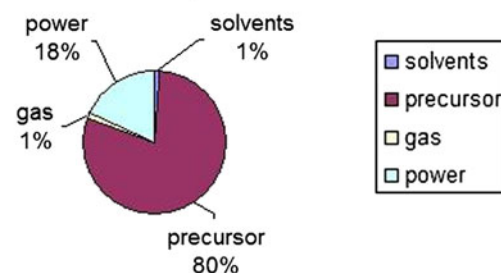


Fig. 23 Bulk scale process costs of RSDT for a 5 \times 5 cell at 75% efficiency

that higher efficiencies can be achieved by enclosing the reactive plume in a shrouded environment. The time row represents the total time required to deposit the given electrolyte mass at the specified efficiency.

It should be noted that a substantial amount of the cost at lab levels is due to the use of oxygen in the process. We are investigating the possibility of using compressed air to replace oxygen in the process to mitigate these costs.

5. Conclusion

The range and versatility of aerosol processes for the generation of the powders and films for solid oxide fuel cell applications has expanded greatly in the last few years. Flame-based processing of SOFC materials shows promise as a method for component fabrication. The advantage of this process compared to the plasma spray process is that it can produce a thin and dense electrolyte layer and has a much better control of the electrode porosity. The flame process can be divided into two categories: aerosol flame deposition where the particles are produced from droplets entering into flame, and gas to particle deposition where the particles form from individual atoms and molecules in the gas phase. Morphological control, fast growth kinetics, and low capital costs suggest that this processing route may hold promise for some if not all deposition layers of SOFC materials.

Table 4 Cost of RSDT process based on approximate lab scale cost for making a $5 \times 5 \text{ cm}^2$ or a 1 m^2 samarium-doped ceria electrolyte

| | 75% Deposition efficiency | | 100% Deposition efficiency | |
|--|---------------------------|------------|----------------------------|------------|
| | 25 | 10000 | 25 | 10000 |
| Cell area, cm^2 | 5 | 5 | 5 | 5 |
| SDC electrolyte thickness, μm | 0.119 | 48.175 | 0.089 | 35.746 |
| theoretical mass electrolyte, g | 0.004 | 0.004 | 0.004 | 0.004 |
| Flow rate, L/min | 75 | 75 | 100 | 100 |
| Assumed efficiency, % | 21 | 8533.83 | 15.83 | 6332.18 |
| Time, min | 0.01 | 0.01 | 0.01 | 0.01 |
| Concentration, mol/L | \$3.75 | \$1,517.53 | \$2.81 | \$1,126.02 |
| Cost/deposition lab scale, \$ | \$0.23 | \$94.69 | \$0.18 | \$70.26 |
| Cost/deposition bulk, \$ | \$92.00 | \$94.69 | \$70.26 | \$70.26 |
| Cost bulk, $\$/\text{m}^2$ | \$19.37 | \$19.93 | \$14.79 | \$14.79 |
| Cost bulk, $\$/\text{kW}$, of electrolyte (a) | | | | |

(a) Baseline power density 475 (mW/cm^2)
 Assumptions:
 \$500/kg SDC precursors
 75 or 100% efficiency
 bulk prices also reflect replacement of oxygen with compressed air

The morphology of the deposited layer is mostly influenced by the nature of precursors, solvents, concentration, flame composition, flame temperature, deposition rate, substrate temperature, and distance of the flame to substrate and of the quenching mechanism. In general, a higher concentration of solution and higher flow rate generate more porous layers. The technology has been brought to the point where controllable and reproducible microstructures can be obtained for different materials, with various feedstock chemistries. By selection of the raw material, solvent chemistry, concentration, flow rate, temperature and type of flame, different porous, and/or dense multicomponent structures can be formed. This provides evidence of both the flexibility and the potential of the technique. In particular, the ability to obtain identical microstructures starting from very different chemistries just by adequately tuning the instrument's parameters is a major breakthrough and justifies further efforts. From this perspective, RSDT has proved to possess the same degree of flexibility usually associated with traditional technologies as screen printing. Also worth mentioning is that RSDT may appear to be a more complex instrument than traditional processing techniques. However, if we consider that no post-thermal processing is required for RSDT coatings and the as-coated materials show very good performance with no further processing, then RSDT is no more complicated than a screen printer combined with a sintering furnace.

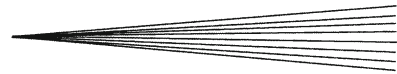
From the material point of view, optimization of the low temperature SOFCs will require more detailed examination of the relationship between processing, microstructure, and properties for the deposition. In particular, a better understanding of segregation and the

behavior of grain boundaries in the electrolyte is required. The mixed oxide composite cathode and anodes are also likely to provide an appropriate material solution for low temperature SOFC. However, interpretation of the porosity effects, nature of the nanostructured surface, and a quantitative interpretation of behavior in terms of the relevant k (the surface exchange coefficient) and D (oxygen self-diffusion coefficient) is required. Further modeling studies substantiated by experiments are required on nucleation, agglomeration, and morphology evolution of porous and dense film under realistic and practical conditions of materials processing.

The industrial priorities are obviously focused on more mature technologies such as screen printing and tape casting; the performance and cost issues of the next generation of low temperature SOFC should be addressed by looking for a broader range of technologies that can make novel structures and have a greater flexibility in materials selection. Research to develop flame-based processing techniques and then integration of multiple SOFC layers by the same process on a metal support are avenues for future study. Finally, emphasis needs to be placed on scale up of flame-based processes to larger levels of production of films while maintaining quality.

References

1. H. Zhu and R.J. Kee, Thermodynamics of SOFC Efficiency and Fuel Utilization as Functions of Fuel Mixtures and Operating Conditions, *J. Power Sour.*, 2006, **161**(2), p 957-964
2. D. Larrain, J. Van Herle, and D. Favrat, Simulation of SOFC Stack and Repeat Elements Including Interconnect Degradation and Anode Reoxidation Risk, *J. Power Sour.*, 2006, **161**(1), p 392-403
3. J.W. Fergus, Effect of Cathode and Electrolyte Transport Properties on Chromium Poisoning in Solid Oxide Fuel Cells, *Int. J. Hydrogen Energy*, 2007, **32**(16), p 3664-3671
4. B.C.H. Steele, Materials for IT-SOFC Stacks: 35 Years R&D: The Inevitability of Gradualness?, *Solid State Ionics*, 2000, **134**(1-2), p 3-20
5. T. Wen, D. Wang, M. Chen, H. Tu, Z. Lu, Z. Zhang, H. Nie, and W. Huang, Material Research for Planar SOFC Stack, *Solid State Ionics*, 2002, **148**(3-4), p 513-519
6. F.J. Gardner, M.J. Day, N.P. Brandon, M.N. Pashley, and M. Cassidy, SOFC Technology Development at Rolls-Royce, *J. Power Sour.*, 2000, **86**(1-2), p 122-129
7. X. Zhang, M. Robertson, C. Decès-Petit, Y. Xie, R. Hui, S. Yick, E. Styles, J. Roller, O. Kesler, R. Maric, and D. Ghosh, NiO-YSZ Cermet Supported Low Temperature Solid Oxide Fuel Cells, *J. Power Sour.*, 2006, **161**(1), p 301-307
8. E. Ivers-Tiffée, A. Weber, and D. Herbristrit, Materials and Technologies for SOFC-Components, *J. Eur. Ceram. Soc.*, 2001, **21**(10-11), p 1805-1811
9. N. Sakai, T. Horita, K. Yamaji, Y.P. Xiong, H. Kishimoto, M.E. Brito, and H. Yokokawa, Material Transport and Degradation Behavior of SOFC Interconnects, *Solid State Ionics*, 2006, **177**(19-25), p 1933-1939
10. T. Inagaki, K. Miura, H. Yoshida, R. Maric, S. Ohara, X. Zhang, K. Mukai, and T. Fukui, High-Performance Electrodes for Reduced Temperature Solid Oxide Fuel Cells with Doped Lanthanum Gallate Electrolyte: II. La(Sr)CoO₃ Cathode, *J. Power Sour.*, 2000, **86**(1-2), p 347-351
11. R. Maric, R. Neagu, Y. Zhang-Steenwinkel, F.P.F. van Berkel, and B. Rietveld, Reactive Spray Deposition Technology—A One-Step Deposition Technique for Solid Oxide Fuel Cell Barrier Layers, *J. Power Sour.*, 2010, **195**(24), p 8198-8201



12. T. Hatae, N. Kakuda, T. Taniyama, and Y. Yamazaki, Low Temperature Preparation and Performance of Ni/YSZ Anode with a Multi-Layered Structure for SOFC, *J. Power Sour.*, 2004, **135**(1-2), p 25-28
13. J.P.P. Huijsmans, F.P.F. van Berkel, and G.M. Christie, Intermediate Temperature SOFC—A Promise for the 21st Century, *J. Power Sour.*, 1998, **71**(1-2), p 107-110
14. S. Hui, D. Yang, Z. Wang, S. Yick, C. Decès-Petit, W. Qi, A. Tuck, R. Maric, and D. Ghosh, Metal-Supported Solid Oxide Fuel Cell Operated at 400-600 °C, *J. Power Sour.*, 2007, **167**(2), p 336-339
15. Z. Wang, J.O. Berghaus, S. Yick, C. Decès-Petit, W. Qu, R. Hui, R. Maric, and D. Ghosh, Dynamic Evaluation of Low-Temperature Metal-Supported Solid Oxide Fuel Cell Oriented to Auxiliary Power Units, *J. Power Sour.*, 2008, **176**(1), p 90-95
16. J. Lee, H. Moon, H. Lee, J. Kim, J. Kim, and K. Yoon, Quantitative Analysis of Microstructure and its Related Electrical Property of SOFC Anode, Ni-YSZ Cermet, *Solid State Ionics*, 2002, **148**(1-2), p 15-26
17. X. Zhang, M. Robertson, S. Yick, C. Decès-Petit, E. Styles, W. Qu, Y. Xie, R. Hui, J. Roller, O. Kesler, R. Maric, and D. Ghosh, $\text{Sm}_{0.5}\text{Sr}_{0.5}\text{CoO}_3 + \text{Sm}_{0.2}\text{Ce}_{0.8}\text{O}_{1.9}$ Composite Cathode for Cermet Supported Thin $\text{Sm}_{0.2}\text{Ce}_{0.8}\text{O}_{1.9}$ Electrolyte SOFC Operating Below 600 °C, *J. Power Sour.*, 2006, **160**(2), p 1211-1216
18. N.M. Sammes and Z. Cai, Ionic Conductivity of Ceria/Yttria Stabilized Zirconia Electrolyte Materials, *Solid State Ionics*, 1997, **100**(1-2), p 39-44
19. K.V. Galloway and N.M. Sammes, Fuel Cells-Solid Oxide Fuel Cells/Anodes, *Encyclopedia of Electrochemical Power Sources*, J. Garche, Ed., Elsevier, Amsterdam, 2009, p 17-24
20. S. Hui, J. Roller, S. Yick, X. Zhang, C. Decès-Petit, Y. Xie, R. Maric, and D. Ghosh, A Brief Review of the Ionic Conductivity Enhancement for Selected Oxide Electrolytes, *J. Power Sour.*, 2007, **172**(2), p 493-502
21. I. Kosacki, H.U. Anderson, Y. Mizutani, and K. Ukai, Nonstoichiometry and Electrical Transport in Sc-Doped Zirconia, *Solid State Ionics*, 2002, **152-153**, p 431-438
22. X. Zhang, M. Robertson, C. Decès-Petit, W. Qu, O. Kesler, R. Maric, and D. Ghosh, Internal Shorting and Fuel Loss of a Low Temperature Solid Oxide Fuel Cell with SDC Electrolyte, *J. Power Sour.*, 2007, **164**(2), p 668-677
23. S. Carter, A. Selcuk, R.J. Chater, J. Kajda, J.A. Kilner, and B.C.H. Steele, Oxygen Transport in Selected Nonstoichiometric Perovskite-Structure Oxides, Part 1, *Solid State Ionics*, 1992, **53-56**, p 597-605
24. B.C.H. Steele, Behavior of Porous Cathodes in High Temperature Fuel Cells, *Solid State Ionics*, 1997, **94**(1-4), p 239-248
25. M.T. Colomer, B.C.H. Steele, and J.A. Kilner, Structural and Electrochemical Properties of the $\text{Sr}_{0.8}\text{Ce}_{0.1}\text{Fe}_{0.7}\text{Co}_{0.3}\text{O}_{3-\delta}$ Perovskite as Cathode Material for ITSOFCs, *Solid State Ionics*, 2002, **147**(1-2), p 41-48
26. B.C.H. Steele and J. Bae, Properties of $\text{La}_{0.6}\text{Sr}_{0.4}\text{Co}_{0.2}\text{Fe}_{0.8}\text{O}_{3-x}$ (LSCF) Double Layer Cathodes on Gadolinium-Doped Cerium Oxide (CGO) Electrolytes: II. Role of Oxygen Exchange and Diffusion, *Solid State Ionics*, 1998, **106**(3-4), p 255-261
27. J.R. Wilson, D.T. Schwartz, and S.B. Adler, Nonlinear Electrochemical Impedance Spectroscopy for Solid Oxide Fuel Cell Cathode Materials, *Electrochim. Acta*, 2006, **51**(8-9), p 1389-1402
28. P. Charpentier, P. Fragnaud, D.M. Schleich, and E. Gehain, Preparation of Thin Film SOFCs Working at Reduced Temperature, *Solid State Ionics*, 2000, **135**(1-4), p 373-380
29. M. Brandner, M. Bram, J. Froitzheim, H.P. Buchkremer, and D. Stöver, Electrically Conductive Diffusion Barrier Layers for Metal-Supported SOFC, *Solid State Ionics*, 2008, **179**(27-32), p 1501-1504
30. Y.B. Matus, L.C. De Jonghe, C.P. Jacobson, and S.J. Visco, Metal-supported Solid Oxide Fuel Cell Membranes for Rapid Thermal Cycling, *Solid State Ionics*, 2005, **176**(5-6), p 443-449
31. H.J. Cho and G.M. Choi, Fabrication and Characterization of Ni-Supported Solid Oxide Fuel Cell, *Solid State Ionics*, 2009, **180**(11-13), p 792-795
32. M. Haldane and T. Etsell, Fabrication of Composite SOFC Anodes Using Polarized Electrochemical Vapor Deposition, *Fuel Cells Bull.*, 2005, **2005**(7), p 12-16
33. K.C. Wincewicz and J.S. Cooper, Taxonomies of SOFC Material and Manufacturing Alternatives, *J. Power Sour.*, 2005, **140**(2), p 280-296
34. G. Schiller, R.H. Henne, M. Lang, R. Ruckdäschel, and S. Schaper, Development of Vacuum Plasma Sprayed Thin-Film SOFC for Reduced Operating Temperature, *Fuel Cells Bull.*, 2000, **3**(21), p 7-12
35. S. Charojrochkul, K.L. Choy, and B.C.H. Steele, Flame Assisted Vapor Deposition of Cathode for Solid oxide Fuel Cells. 1. Microstructure Control from Processing Parameters, *J. Eur. Ceram. Soc.*, 2004, **24**(8), p 2515-2526
36. D. Beckel, A. Bieberle-Hütter, A. Harvey, A. Infortuna, U.P. Muecke, M. Prestat, J.L.M. Rupp, and L.J. Gauckler, Thin Films for Micro Solid Oxide Fuel Cells, *J. Power Sour.*, 2007, **173**(1), p 325-345
37. R. Hui, Z. Wang, O. Kesler, L. Rose, J. Jankovic, S. Yick, R. Maric, and D. Ghosh, Thermal plasma spraying for SOFCs: Applications, Potential Advantages, and Challenges, *J. Power Sour.*, 2007, **170**(2), p 308-323
38. C. Li, C. Li, and X. Ning, Performance of YSZ Electrolyte Layer Deposited by Atmospheric Plasma Spraying for Cermet-Supported Tubular SOFC, *Vacuum*, 2004, **73**(3-4), p 699-703
39. C. Li, C. Li, H. Long, Y. Xing, X. Ning, C. Zhang, H. Liao, and C. Coddet, Characterization of Atmospheric Plasma-Sprayed $\text{Se}_2\text{O}_3\text{-ZrO}_2$ Electrolyte Coating, *Solid State Ionics*, 2006, **177**(19-25), p 2149-2153
40. G. Mauer, R. Vaßen, and D. Stöver, Atmospheric Plasma Spraying of Yttria-Stabilized Zirconia Coatings with Specific Porosity, *Surf. Coat. Technol.*, 2009, **204**(1-2), p 172-179
41. R. Henne, Solid Oxide Fuel Cells: A Challenge for Plasma Deposition Processes, *J. Thermal Spray Technol.*, 2007, **16**(3), p 381-403
42. R. Hui, J.O. Berghaus, C. Decès-Petit, W. Qu, S. Yick, J. Legoux, and C. Moreau, High Performance Metal-Supported Solid Oxide Fuel Cells Fabricated by Thermal Spray, *J. Power Sour.*, 2009, **191**(2), p 371-376
43. D. Perednis, Y. Xie, X. Zhang, and D. Ghosh, Deposition of Samaria-Doped Ceria Electrolyte Using Spray Pyrolysis, *Electrochim. Soc.*, 2006, **501**(30), p 1092
44. D. Perednis, Y. Xie, X. Zhang, D. Ghosh, R. Maric, and J. Roller, Solid Oxide Fuel Cells with Samaria-Doped Ceria Electrolytes Prepared Via Spray Pyrolysis, *Proceedings of 1st International Symposium on Fuel Cell and Hydrogen Technologies, COM2005*, August 21-24, Calgary, Canada, 2005, p 273
45. D. Perednis and L.J. Gauckler, Solid Oxide Fuel Cells with Electrolytes Prepared Via Spray Pyrolysis, *Solid State Ionics*, 2004, **166**(3-4), p 229-239
46. A.O. Stoermer, J.L.M. Rupp, and L.J. Gauckler, Spray Pyrolysis of Electrolyte Interlayers for Vacuum Plasma-Sprayed SOFC, *Solid State Ionics*, 2006, **177**(19-25), p 2075-2079
47. J. Will, A. Mitterdorfer, C. Kleinlogel, D. Perednis, and L.J. Gauckler, Fabrication of Thin Electrolytes for Second-Generation Solid Oxide Fuel Cells, *Solid State Ionics*, 2000, **131**(1-2), p 79-96
48. J. Roller, "Low Platinum Electrodes for Proton Exchange Fuel Cells Manufactured by Reactive Spray Deposition Technology, 2009," Masters Thesis Defense, University of British Columbia
49. R. Neagu, X. Zhang, R. Maric, and J.M. Roller, Characterization and Performance of SOFC Components Made by Reactive Spray Deposition Technology, *Electrochim. Soc.*, 2009, **902**(12), p 1357
50. M. van Tuel, F. van Berke, B. Rietveld, R. Maric, S. Uhlenbruck, F. Tietz, Modification of Cell Microstructure and Compositions for High and Stable Performance of Low Temperature SOFC's, *European Fuel Cell Forum 2009*, 2009
51. R. Strobel and S.E. Pratsinis, Direct Synthesis of Maghemite, Magnetite and Wustite Nanoparticles by Flame Spray Pyrolysis, *Adv. Powder Technol.*, 2009, **20**(2), p 190-194
52. M. Aromaa, H. Keskinen, and J.M. Mäkelä, The Effect of Process Parameters on the Liquid Flame Spray Generated Titania Nanoparticles, *Biomol. Eng.*, 2007, **24**(5), p 543-548
53. G. Bolelli, V. Cannillo, R. Gadow, A. Killinger, L. Lusvardi, J. Rauch, and M. Romagnoli, Effect of the Suspension Composition on the Microstructural Properties of High Velocity Suspension Flame Sprayed (HVSFS) Al_2O_3 Coatings, *Surf. Coat. Technol.*, 2010, **204**(8), p 1163-1179

54. A. Killinger, M. Kuhn, and R. Gadow, High-Velocity Suspension Flame Spraying (HVSFS), A New Approach for Spraying Nanoparticles with Hypersonic Speed, *Surf. Coat. Technol.*, 2006, **201**(5), p 1922-1929
55. C. Monterrubio-Badillo, H. Ageorges, T. Chartier, J.F. Coudert, and P. Fauchais, Preparation of LaMnO₃ Perovskite Thin Films by Suspension Plasma Spraying for SOFC Cathodes, *Surf. Coat. Technol.*, 2006, **200**(12-13), p 3743-3756
56. A.R. Nicoll, A. Salito, and K. Honegger, The Potential of Plasma Spraying for the Deposition of Coatings on SOFC Components, *Solid State Ionics*, 1992, **52**(1-3), p 269-275
57. C. Li, C. Li, and L. Guo, Effect of Composition of NiO/YSZ Anode on the Polarization Characteristics of SOFC Fabricated by Atmospheric Plasma Spraying, *Int. J. Hydrogen Energy*, 2010, **35**(7), p 2964-2969
58. B.D. White, O. Kesler, and L. Rose, Air Plasma Spray Processing and Electrochemical Characterization of SOFC Composite Cathodes, *J. Power Sour.*, 2008, **178**(1), p 334-343
59. N.I. Karageorgakis, A. Heel, T. Graule, and L.J. Gauckler, Flame Spray Deposition of Nanocrystalline Dense Ce_{0.8}Gd_{0.2}O_{2-δ} Thin Films: Deposition Mechanism and Microstructural Characterization, *Solid State Ionics*, 2010, in press, corrected proof
60. A. Heel, P. Holtappels, and T. Graule, On the Synthesis and Performance of Flame-Made Nanoscale La_{0.6}Sr_{0.4}CoO_{3-δ} and its Influence on the Application as an Intermediate Temperature Solid Oxide Fuel Cell Cathode, *J. Power Sour.*, 2010, **195**(19), p 6709-6718
61. J.M. Im, H.J. You, Y.S. Yoon, and D.W. Shin, Synthesis of Nano-Sized Gadolinia Doped Ceria Powder by Aerosol Flame Deposition, *J. Eur. Ceram. Soc.*, 2007, **27**(13-15), p 3671-3675
62. H. You, K. Cho, Y. Yoon, J. Im, and D. Shin, Synthesis of Yttria-Stabilized Zirconia Film by Aerosol Flame Pyrolysis Deposition, *J. Anal. Appl. Pyrol.*, 2008, **81**(1), p 14-19
63. S. Charojrochkul, R.M. Lothian, K.L. Choy, and B.C.H. Steele, Flame Assisted Vapor Deposition of Cathode for Solid Oxide Fuel Cells. 2. Modeling of Processing Parameters, *J. Eur. Ceram. Soc.*, 2004, **24**(8), p 2527-2535
64. P. Bohac and L. Gauckler, Chemical Spray Deposition of YSZ and GCO Solid Electrolyte Films, *Solid State Ionics*, 1999, **119**(1-4), p 317-321
65. J.M. Im, H.J. You, Y.S. Yoon, and D.W. Shin, Synthesis of Nano-Crystalline Gd_{0.1}Ce_{0.9}O_{2-x} for IT-SOFC by Aerosol Flame Deposition, *Ceram. Int.*, 2008, **34**(4), p 877-881
66. N.I. Karageorgakis, A. Heel, A. Bieberle-Hütter, J.L.M. Rupp, T. Graule, and L.J. Gauckler, Flame Spray Deposition of La_{0.6}Sr_{0.4}CoO_{3-δ} Thin Films: Microstructural Characterization, Electrochemical Performance and Degradation, *J. Power Sour.*, 2010, **195**(24), p 8152-8161
67. A. Naidja, C.R. Krishna, T. Butcher, and D. Mahajan, Cool Flame Partial Oxidation and its Role in Combustion and Reforming of Fuels for Fuel Cell Systems, *Prog. Energy Combust. Sci.*, 2003, **29**(2), p 155-191
68. K. Wang, P. Zeng, and J. Ahn, High Performance Direct Flame Fuel Cell Using A Propane Flame, *Proc. Combust. Inst.*, 2011, **33**(2), p 3431-3437
69. S. Charojrochkul, K. Choy, and B.C.H. Steele, Cathode/Electrolyte Systems for Solid Oxide Fuel Cells Fabricated Using Flame Assisted Vapor deposition technique, *Solid State Ionics*, 1999, **121**(1-4), p 107-113
70. G. Meng, H. Song, Q. Dong, and D. Peng, Application of Novel Aerosol-Assisted Chemical Vapor Deposition Techniques for SOFC Thin Films, *Solid State Ionics*, 2004, **175**(1-4), p 29-34
71. H. Song, C. Xia, G. Meng, and D. Peng, Preparation of Gd₂O₃ Doped CeO₂ Thin Films by Oxy-Acetylene Combustion Assisted Aerosol-Chemical Vapor Deposition Technique on Various Substrates and Zone Model for Microstructure, *Thin Solid Films*, 2003, **434**(1-2), p 244-249
72. Z. Xu, J. Sankar, and S. Yarmolenko, Yttria-Stabilized Zirconia Coatings Produced Using Combustion Chemical Vapor Deposition, *Surf. Coat. Technol.*, 2004, **177-178**, p 52-59
73. Y. Liu, C. Compson, and M. Liu, Nanostructured and Functionally Graded Cathodes for Intermediate-Temperature SOFCs, *Fuel Cells Bull.*, 2004, **2004**(10), p 12-15
74. A.T. Hunt, W.B. Carter, and J.K., Cochran, Jr., Combustion Chemical Vapor Deposition: A Novel Thin-Film Deposition Technique, *Appl. Phys. Lett.*, 1993, **63**(2), p 266-268
75. R. Strobel, A. Alfons, and S.E. Pratsinis, Aerosol Flame Synthesis of Catalysts, *Adv. Powder Technol.*, 2006, **17**(5), p 457-480
76. R. Maric, J.M. Roller, R. Neagu, K. Fatih, and A. Tuck, Low Pt Thin Cathode Layer Catalyst Layer by Reactive Spray Deposition Technology, *ECS Trans*, 2008, **12**(1), p 59-63
77. R. Maric, S. Seward, P. Faguy, and M. Oljaca, Electrolyte Materials for Intermediate Temperature Fuel Cells Produced via Combustion Chemical Vapor Condensation, *Electrochem. Solid-State Lett.*, 2003, **6**(5), p A91-A95
78. W.B. Carter, G.W. Book, T.A. Polley, D.W. Stollberg, and J.M. Hampikian, Combustion Chemical Vapor Deposition of CeO₂ Film, *Thin Solid Films*, 1999, **347**(1-2), p 25-30
79. Y.S. Yoon, J.M. Im, and D.W. Shin, Microstructure and Electrical Conductivity of NiO-YSZ Nano-Powder Synthesized by Aerosol Flame Deposition, *Ceram. Int.*, 2008, **34**(4), p 873-876
80. R. Maric, J. Roller, R. Neagu, and F. Khalid, "Catalytic Materials for Fuel Cell Electrodes and Methods for Their Manufacture" PCT/CA2009/001609, 2010
81. R. Maric, J. Roller, and T. Vanderhoeck, "Reactive Spray Formation of Coatings and Powders" PCT/CA2006/001713, 2007
82. K. Kuo, *Principles of Combustion*, Wiley, New York, 1986
83. J.A. Thornton, High Rate Thick Film Growth, *Annu. Rev. Mater. Sci.*, 1977, **7**(1), p 239-260
84. J.A. Thornton, Influence of Apparatus Geometry and Deposition Conditions on the Structure and Topography of Thick Sputtered Coatings, *J. Vac. Sci. Technol.*, 1974, **11**(4), p 666-670
85. T.A. Polley and W.B. Carter, Zone Model for Zinc Oxide Deposited by Combustion Chemical Vapor Deposition, *Thin Solid Films*, 2001, **384**(2), p 177-184
86. Z. Xu, C. Waters, X. Wang, N. Sudhir, S. Yarmolenko, and J. Sankar, Texture and Nano Mechanical Properties of YSZ Electrolyte Thin Films Prepared by CCVD and PLD, *C-MRS Int. Symp. Proc.*, 2003, **778**, p 189
87. S.P.S. Badwal, Electrical Conductivity of Single Crystal and Polycrystalline Yttria-Stabilized Zirconia, *J. Mater. Sci.*, 1984, **19**(6), p 1767-1776
88. Y. Liu, W. Rauch, S. Zha, and M. Liu, Fabrication of Sm_{0.5}Sr_{0.5}CoO_{3-δ}Sm_{0.1}Ce_{0.9}O_{2-δ} Cathodes for Solid Oxide Fuel Cells Using Combustion CVD, *Solid State Ionics*, 2004, **166**(3-4), p 261-268
89. G.L. Messing, S. Zhang, and G.V. Jayanthi, Ceramic Powder Synthesis by Spray Pyrolysis, *J. Am. Ceram. Soc.*, 1993, **76**(11), p 2707-2726
90. R. Neagu, R. Maric, and C. Deces-Petit, Thin Layers of YSZ and GDC Electrolyte Deposited by RSDT, *Hydrogen and Fuel Cells 2009*, May (Vancouver, BC, Canada)
91. A. Mitterdorfer and L.J. Gauckler, La₂Zr₂O₇ Formation and Oxygen Reduction Kinetics of the La_{0.85}Sr_{0.15}MnyO₃, O₂(g)YSZ System, *Solid State Ionics*, 1998, **111**(3-4), p 185-218
92. S.P. Simner, J.P. Shelton, M.D. Anderson, and J.W. Stevenson, Interaction Between La(Sr)FeO₃ SOFC Cathode and YSZ Electrolyte, *Solid State Ionics*, 2003, **161**(1-2), p 11-18
93. B. Schinking, R. Petzold, H. Tiller, and G. Grundmeier, Chemical Structure and Morphology of Ultrathin Combustion CVD Layers on Zinc Coated Steel, *Appl. Surf. Sci.*, 2001, **179**(1-4), p 79-87
94. B. Schinking, R. Petzold, H.-J. Tiller, G. Grundmeier, Chemical Structure and Morphology of Ultra-Thin Combustion CVD Layers on Zinc Coated Steel, *Materials Week 2000 International Congress on Advanced Materials, Processes and Applications*, September 25-28, Munich, Germany, 2000
95. H. Tiller, R. Göbel, W. Kaiser, and H. Kleinert, Ed., *DECHEMA Monographienband*, VCH Verlagsgesellschaft, Weinheim, 1990, p 95
96. H. Tiller, R. Göbel, B. Magnus, A. Garschke, and R. Musil, A New Concept of Metal-Resin Adhesion Using an Intermediate Layer of SiO_x-C, *Thin Solid Films*, 1989, **169**(1), p 159-168
97. E. Carlson, Y. Yanf, and C. Fulton, *Solid Oxide Fuel Cell Manufacturing Cost Model: Simulating Relationships between Performance, Manufacturing, and Cost of Production*, 2004, DE-FC26-02NT41568